

Search for narrow and broad dijet resonances in proton-proton collisions at $\sqrt{s} = 13$ TeV and constraints on dark matter mediators and other new particles

The CMS Collaboration*

Abstract

Searches for resonances decaying into pairs of jets are performed using proton-proton collision data collected at $\sqrt{s} = 13$ TeV corresponding to an integrated luminosity of up to 36 fb^{-1} . A low-mass search, for resonances with masses between 0.6 and 1.6 TeV, is performed based on events with dijets reconstructed at the trigger level from calorimeter information. A high-mass search, for resonances with masses above 1.6 TeV, is performed using dijets reconstructed offline with a particle-flow algorithm. The dijet mass spectrum is well described by a smooth parameterization and no evidence for the production of new particles is observed. Upper limits at 95% confidence level are reported on the production cross section for narrow resonances with masses above 0.6 TeV. In the context of specific models, the limits exclude string resonances with masses below 7.7 TeV, scalar diquarks below 7.2 TeV, axigluons and colorons below 6.1 TeV, excited quarks below 6.0 TeV, color-octet scalars below 3.4 TeV, W' bosons below 3.3 TeV, Z' bosons below 2.7 TeV, Randall–Sundrum gravitons below 1.8 TeV and in the range 1.9 to 2.5 TeV, and dark matter mediators below 2.6 TeV. The limits on both vector and axial-vector mediators, in a simplified model of interactions between quarks and dark matter particles, are presented as functions of dark matter particle mass and coupling to quarks. Searches are also presented for broad resonances, including for the first time spin-1 resonances with intrinsic widths as large as 30% of the resonance mass. The broad resonance search improves and extends the exclusions of a dark matter mediator to larger values of its mass and coupling to quarks.

Submitted to the Journal of High Energy Physics

1 Introduction

Models of physics that extend the standard model (SM) often require new particles that couple to quarks (q) and/or gluons (g) and decay to dijets. The natural width of resonances in the dijet mass (m_{jj}) spectrum increases with the coupling, and may vary from narrow to broad compared to the experimental resolution. For example, in a model in which dark matter (DM) particles couple to quarks through a DM mediator, the mediator can decay to either a pair of DM particles or a pair of jets and therefore can be observed as a dijet resonance [1] that is either narrow or broad, depending on the strength of the coupling. When the resonance is broad, its observed line-shape depends significantly on the resonance spin. Here we report a search for narrow dijet resonances and a complementary search for broad resonances that considers multiple values of the resonance spin and widths as large as 30% of the resonance mass. Both approaches are sensitive to resonances with intrinsic widths that are small compared to the experimental resolution, but the broad resonance search is also sensitive to resonances with larger intrinsic widths. We explore the implications for multiple specific models of dijet resonances and for a range of quark coupling strength for a DM mediator.

1.1 Searches

This paper presents the results of searches for dijet resonances that were performed with proton-proton (pp) collision data collected at $\sqrt{s} = 13$ TeV. The data correspond to an integrated luminosity of up to 36 fb^{-1} and were collected in 2016 with the CMS detector at the CERN LHC. Similar searches for narrow resonances have been published previously by the ATLAS and CMS Collaborations at $\sqrt{s} = 13$ TeV [2–6], 8 TeV [7–10], and 7 TeV [11–17] using strategies reviewed in Ref. [18]. A search for broad resonances considering natural widths as large as 30% of the resonance mass, directly applicable to spin-2 resonances only, has been published once before by CMS at $\sqrt{s} = 8$ TeV [8]. Here we explicitly consider spin-1 and spin-2 resonances that are both broad.

The narrow resonance search is conducted in two regions of the dijet mass. The first is a low-mass search for resonances with masses between 0.6 and 1.6 TeV. This search uses a dijet event sample corresponding to an integrated luminosity of 27 fb^{-1} , less than the full data sample, as discussed in Section 2.3. The events are reconstructed, selected, and recorded in a compact form by the high-level trigger (HLT) in a technique referred to as “data scouting” [19]. Data scouting was previously used for low-mass searches published by CMS at $\sqrt{s} = 13$ TeV [4] and at 8 TeV [7], and is similar to a trigger-level search at 13 TeV recently published by ATLAS [2]. The second search is a high-mass search [3–6, 8–17] for resonances with masses above 1.6 TeV, based on dijet events that are reconstructed offline in the full data sample corresponding to an integrated luminosity of 36 fb^{-1} . The search for broad resonances uses the same selected events as does the high-mass search for narrow resonances.

1.2 Models

We present model independent results for s -channel dijet resonances and apply the results to the following narrow dijet resonances predicted by eleven benchmark models:

1. String resonances [20, 21], which are the Regge excitations of the quarks and gluons in string theory. There are multiple mass-degenerate states with various spin and color multiplicities. The qg states dominate the cross section for all masses considered.
2. Scalar diquarks, which decay to qq and $\bar{q}\bar{q}$, predicted by a grand unified theory based on the E_6 gauge symmetry group [22]. The coupling constant is conventionally assumed to

be of electromagnetic strength.

3. Mass-degenerate excited quarks (q^*), which decay to qg , predicted in quark compositeness models [23, 24]; the compositeness scale is set to be equal to the mass of the excited quark.
- 4–5. Axigluons and colorons, axial-vector and vector particles, which are predicted in the chiral color [25] and the flavor-universal coloron [26] models, respectively. These are massive color-octet particles, which decay to $q\bar{q}$. The coloron coupling parameter is set at its minimum value $\cot\theta = 1$ [26], which gives identical production cross section values for colorons and axigluons.
6. Color-octet scalars [27], which decay to gg , appear in dynamical electroweak symmetry breaking models such as technicolor. The value of the squared anomalous coupling of color-octet scalars to gluons is chosen to be $k_s^2 = 1/2$ [28].
- 7–8. New gauge bosons (W' and Z'), which decay to $q\bar{q}$, predicted by models that include new gauge symmetries [29]; the W' and Z' bosons are assumed to have standard-model-like couplings.
9. Randall–Sundrum (RS) gravitons (G), which decay to $q\bar{q}$ and gg , predicted in the RS model of extra dimensions [30]. The value of the dimensionless coupling k/\bar{M}_{Pl} is chosen to be 0.1, where k is the curvature scale and \bar{M}_{Pl} is the reduced Planck mass.
10. Dark matter mediators, which decay to $q\bar{q}$ and pairs of DM particles, are the mediators of an interaction between quarks and dark matter [31, 32]. For the DM mediator we follow the recommendations of Ref. [31] on the model choice and coupling values, using a simplified model [32] of a spin-1 mediator decaying only to $q\bar{q}$ and pairs of DM particles, with an unknown mass m_{DM} , and with a universal quark coupling $g_q = 0.25$ and a DM coupling $g_{\text{DM}} = 1.0$.
11. Leptophobic Z' resonances [33], which decay to $q\bar{q}$ only, with a universal quark coupling g'_q related to the coupling of Ref. [33] by $g'_q = g_B/6$.

2 Measurement

2.1 Detector

A detailed description of the CMS detector and its coordinate system, including definitions of the azimuthal angle ϕ (in radians) and pseudorapidity variable η , is given in Ref. [34]. The central feature of the CMS apparatus is a superconducting solenoid of 6 m internal diameter providing an axial field of 3.8 T. Within the solenoid volume are located the silicon pixel and strip tracker ($|\eta| < 2.4$) and the barrel and endcap calorimeters ($|\eta| < 3.0$), consisting of a lead tungstate crystal electromagnetic calorimeter, and a brass and scintillator hadron calorimeter. An iron and quartz-fiber hadron forward calorimeter is located in the region ($3.0 < |\eta| < 5.0$), outside the solenoid volume.

2.2 Jet reconstruction

A particle-flow (PF) event algorithm is used to reconstruct and identify each individual particle with an optimized combination of information from the various elements of the CMS detector [35]. Particles are classified as muons, electrons, photons, and either charged or neutral hadrons. Jets are reconstructed either using the PF algorithm, yielding “PF-jets”, or from

energy deposits in the calorimeters, yielding “Calo-jets”. The PF-jets, reconstructed offline, are used for the high-mass search, while Calo-jets, reconstructed at the HLT, are used for the low-mass search. To reconstruct either type of jet, we use the anti- k_T algorithm [36, 37] with a distance parameter of 0.4, as implemented in the FASTJET package [38]. For the high-mass search, at least one reconstructed vertex is required. The reconstructed vertex with the largest value of summed physics-object p_T^2 is taken to be the primary pp interaction vertex. Here the physics objects are the jets made of tracks, clustered using the jet finding algorithm [37, 38] with the tracks assigned to the vertex as inputs, and the associated missing transverse momentum, taken as the negative vector sum of the p_T of those jets. For PF-jets, charged PF candidates not originating from the primary vertex are removed prior to the jet finding. For both PF-jets and Calo-jets, an event-by-event correction based on the jet area [39, 40] is applied to the jet energy to remove the estimated contribution from additional collisions in the same or adjacent bunch crossings (pileup).

2.3 Trigger and minimum dijet mass

Events are selected using a two-tier trigger system [41]. Events satisfying loose jet requirements at the first level (L1) trigger are examined by the HLT. We use single-jet triggers that require a jet in the event to satisfy a predefined p_T threshold. We also use triggers that require H_T to exceed a predefined threshold, where H_T is the scalar sum of the p_T of all jets in the event with $|\eta| < 3.0$.

For the high-mass search, the full event information is reconstructed if the event satisfies the HLT trigger. In the early part of the data taking period, the HLT trigger required $H_T > 800$ GeV, with H_T calculated using PF-jets with $p_T > 30$ GeV. For the remainder of the run, an HLT requiring $H_T > 900$ GeV with this same jet p_T threshold was used. The latter H_T trigger suffered from an inefficiency. The efficiency loss occurred within the H_T trigger at L1, towards the end of the data taking period used in this analysis. To recover the lost efficiency we used single-jet triggers at the HLT that did not rely on the H_T trigger at L1 but instead used an efficient single-jet trigger at L1. There were three such triggers at the HLT: the first requiring a PF-jet with $p_T > 500$ GeV, a second requiring a Calo-jet with $p_T > 500$ GeV, and a third requiring a PF-jet with an increased distance parameter of 0.8 and $p_T > 450$ GeV. The trigger used for the high-mass search was the logical OR of these five triggers. We select events with $m_{jj} > 1.25$ TeV, where the dijet mass is fully reconstructed offline using wide jets, defined later. For this selection, the combined L1 trigger and HLT was found to be fully efficient for the full 36 fb^{-1} sample, as shown in Fig. 1. Here the absolute trigger efficiency is measured using a sample acquired with an orthogonal trigger requiring muons with $p_T > 45$ GeV at the HLT.

The data scouting technique is used for the low-mass search. When an event passes a data scouting trigger, the Calo-jets reconstructed at the HLT are saved along with the event energy density and the missing transverse momentum reconstructed from the calorimeter. The energy density is defined for each event as the median calorimeter energy per unit area calculated in a grid of $\eta - \phi$ cells [40] covering the calorimeter acceptance. The shorter time required for the reconstruction of the calorimetric quantities and the reduced size of the data recorded for these events allow a reduced H_T threshold compared to the high-mass search. For the low-mass search, Calo-jets with $p_T > 40$ GeV are used to compute H_T . The trigger threshold is $H_T > 250$ GeV, and we select events with $m_{jj} > 0.49$ TeV for which the trigger is fully efficient, as shown in Fig. 1. Here the trigger efficiency is measured using a prescaled sample acquired with a data scouting trigger which required only that the event passed the jet trigger at L1 with $H_T > 175$ GeV. This L1 trigger is also fully efficient for $m_{jj} > 0.49$ TeV, measured using another prescaled sample acquired with an even looser trigger with effectively no requirements

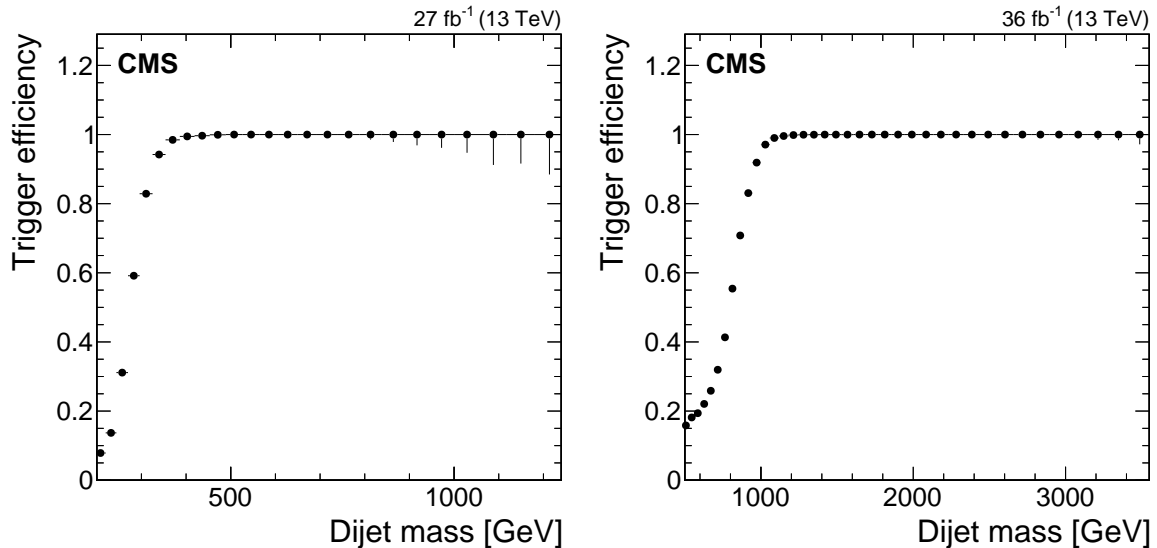


Figure 1: The efficiency of the trigger for the low-mass search (left) and the high-mass search (right) as a function of dijet mass for wide jets, defined in Section 2.5, after all jet calibrations and event selections discussed in Section 2. The horizontal lines on the data points show the variable bin sizes.

(zero-bias) at L1 and requiring at least one Calo-jet with $p_T > 40$ GeV at the HLT. Unlike the high-mass search, there were no single-jet triggers at the HLT in data scouting that would allow for the recovery of the inefficiency in the L1 trigger in 9 fb^{-1} of data at the end of the run, so only the first 27 fb^{-1} of integrated luminosity was used for the low-mass search.

The trigger efficiencies for the low-mass and high-mass regions are shown as functions of dijet mass in Fig. 1. The binning choices are the same as those adopted for the dijet mass spectra. Fig. 1 illustrates that the searches are fully efficient for the chosen dijet mass thresholds. For the purpose of our search, full efficiency requires the measured trigger inefficiency in a bin to be less than the fractional statistical uncertainty in the number of events in the same bin in the dijet mass spectrum. For example, the measured trigger efficiency in the bin between 1246 and 1313 GeV in Fig. 1 (right) is $99.95 \pm 0.02\%$, giving a trigger inefficiency of 0.05% in that bin, which is less than the statistical uncertainty of 0.08% arising from the 1.6 million events in that same bin of the dijet mass spectrum. This criterion for choosing the dijet mass thresholds, $m_{jj} > 1.25$ TeV for the high mass search and $m_{jj} > 0.49$ TeV for the low mass search, ensures that the search results are not biased by the trigger inefficiency.

2.4 Offline calibration and jet identification

The jet momenta and energies are corrected using calibration constants obtained from simulation, test beam results, and pp collision data at $\sqrt{s} = 13$ TeV. The methods described in Ref. [40] are used and all *in-situ* calibrations are obtained from the current data. All jets, the PF-jets in the high-mass search and Calo-jets in the low-mass search, are required to have $p_T > 30$ GeV and $|\eta| < 2.5$. The two jets with largest p_T are defined as the leading jets. Jet identification (ID) criteria are applied to remove spurious jets associated with calorimeter noise as well as those associated with muon and electron candidates that are either mis-reconstructed or isolated [42]. For all PF-jets, the jet ID requires that the neutral hadron and photon energies are less than 90% of the total jet energy. For PF-jets that satisfy $|\eta| < 2.4$, within the fiducial tracker coverage, the jet ID additionally requires that the jet has non-zero charged hadron energy, and muon and electron energies less than 80 and 90% of the total jet energy, respectively. The jet ID for Calo-

jets requires that the jet be detected by both the electromagnetic and hadron calorimeters with the fraction of jet energy deposited within the electromagnetic calorimeter between 5 and 95% of the total jet energy. An event is rejected if either of the two leading jets fails the jet ID criteria.

2.5 Wide jet reconstruction and event selection

Spatially close jets are combined into “wide jets” and used to determine the dijet mass, as in the previous CMS searches [4, 5, 7, 8, 10, 11, 14]. The wide-jet algorithm, designed for dijet resonance event reconstruction, reduces the analysis sensitivity to gluon radiation from the final-state partons. The two leading jets are used as seeds and the four-vectors of all other jets, if within $\Delta R = \sqrt{(\Delta\eta)^2 + (\Delta\phi)^2} < 1.1$, are added to the nearest leading jet to obtain two wide jets, which then form the dijet system. The dijet mass is the magnitude of the momentum-energy 4-vector of the dijet system, which is the invariant mass of the two wide jets. The wide jet algorithm thereby collects hard gluon radiation, satisfying the jet requirement $p_T > 30$ GeV and found nearby the leading two final state partons, in order to improve the dijet mass resolution. This is preferable to only increasing the distance parameter within the anti- k_T algorithm to 1.1, which would include in the leading jets the unwanted soft energy from pile-up and initial state radiation. The wide jet algorithm is similar to first increasing the distance parameter and then applying jet trimming [43] to remove unwanted soft energy.

The angular distribution of background from t -channel dijet events is similar to that for Rutherford scattering, approximately proportional to $1/[1 - \tanh(|\Delta\eta|/2)]^2$, which peaks at large values of $|\Delta\eta|$. This background is suppressed by requiring the pseudorapidity separation of the two wide jets to satisfy $|\Delta\eta| < 1.3$. This requirement also makes the trigger efficiency in Fig. 1 turn on quickly, reaching a plateau at 100% for relatively low values of dijet mass. This is because the jet p_T threshold of the trigger at a fixed dijet mass is more easily satisfied at low $|\Delta\eta|$, as seen by the approximate relation $m_{jj} \approx 2p_T \cosh(|\Delta\eta|/2)$.

The above requirements maximize the search sensitivity for isotropic decays of dijet resonances in the presence of dijet background from quantum chromodynamics (QCD).

2.6 Calibration of wide jets in the low-mass search

The jet energy scale of the low-mass search has been calibrated to be the same as the jet energy scale of the high-mass search. For the low-mass search, after wide jet reconstruction and event selection, we calibrate the wide jets reconstructed from Calo-jets at the HLT to have the same average response as the wide jets reconstructed from PF-jets. We use a smaller *monitoring* data set, which includes both Calo-jets at the HLT and the fully reconstructed PF-jets, to measure the p_T difference between the two types of wide jets, as shown in Fig. 2. A dijet balance “tag-and-probe” method similar to that discussed in Ref. [40] is used. One of the two jets in the dijet system is designated as the tag jet, and the other is designated as the probe jet, and the p_T difference between Calo-Jets at the HLT and fully reconstructed PF-jets is measured for the probe jet as a function of the p_T of the tag PF-jet. We avoid jet selection bias of the probe Calo-Jet p_T , which would result from resolution effects on the steeply falling p_T spectrum, by measuring the p_T difference as a function of the p_T of the tag PF-jet instead of the p_T of the probe Calo-jet at the HLT. This calibration is then translated into a function of the average p_T of the probe Calo-jets. Figure 2 shows this measurement of the p_T difference, as a function of jet p_T , from the monitoring data set. The measured points are fit with a parameterization and the resulting smooth curve is used to calibrate the wide jets in the low-mass search.

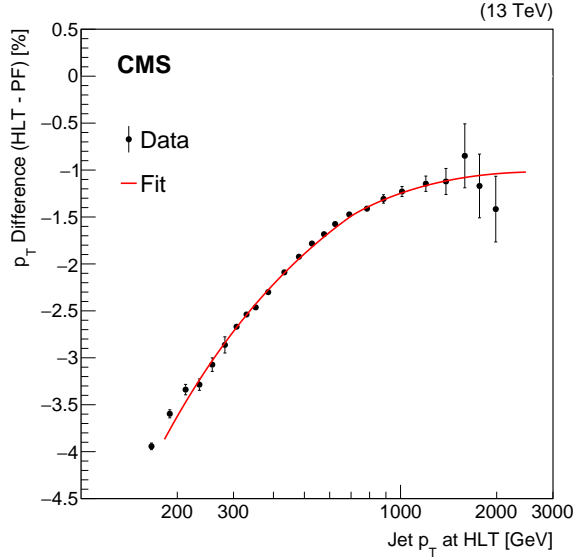


Figure 2: The calibration of jets in the low-mass analysis. The percent difference in data (points), between the p_T of the wide jets reconstructed from Calo-jets at the HLT and the wide jets reconstructed from PF-jets, is fit to a smooth parameterization (curve), as a function of the HLT p_T .

2.7 Dijet data and QCD background predictions

As the dominant background for this analysis is expected to be the QCD production of two or more jets, we begin by performing comparisons of the data to QCD background predictions for the dijet events. The predictions are based upon a sample of 56 million Monte Carlo events produced with the PYTHIA 8.205 [44] program with the CUETP8M1 tune [45, 46] and including a GEANT4-based [47] simulation of the CMS detector. The QCD background predictions are normalized to the data by multiplying them by a factor of 0.87 for the high-mass search and by a factor of 0.96 for the low-mass search, so that for each search the prediction for the total number of events agrees with the number observed. In Fig. 3, we observe that the measured azimuthal separation of the two wide jets, $\Delta\phi$, displays the “back-to-back” distribution expected from QCD dijet production. The strong peak at $\Delta\phi = \pi$, with very few events in the region $\Delta\phi \sim 0$, shows that the data sample is dominated by genuine parton-parton scattering, with negligible backgrounds from detector noise or other nonphysical sources that would produce events more isotropic in $\Delta\phi$. In Fig. 4, we observe that dijet $|\Delta\eta|$ has a distribution dominated by the t -channel parton exchange as does the QCD production of two jets. Note that the production rate increases with increasing $|\Delta\eta|$, whereas s -channel signals from most models of dijet resonances would decrease with increasing $|\Delta\eta|$. In Fig. 5, we observe that the number of dijets produced falls steeply and smoothly as a function of dijet mass. The observed dijet mass distributions are very similar to the QCD prediction from PYTHIA, which includes a leading order QCD calculation and parton shower effects. In Fig. 6, we also compare the dijet mass data to a next-to-leading order (NLO) QCD prediction from POWHEG 2.0 [48] normalized to the data. For this prediction, we used 10 million dijet events from an NLO calculation of two jet production [49] using NNPDF3.0 NLO parton distribution functions [50], interfaced with the aforementioned PYTHIA 8 parton shower and simulation of the CMS detector. The POWHEG prediction models the data better than the PYTHIA prediction does. It is clear from these comparisons that the dijet mass data behaves approximately as expected from QCD predictions.

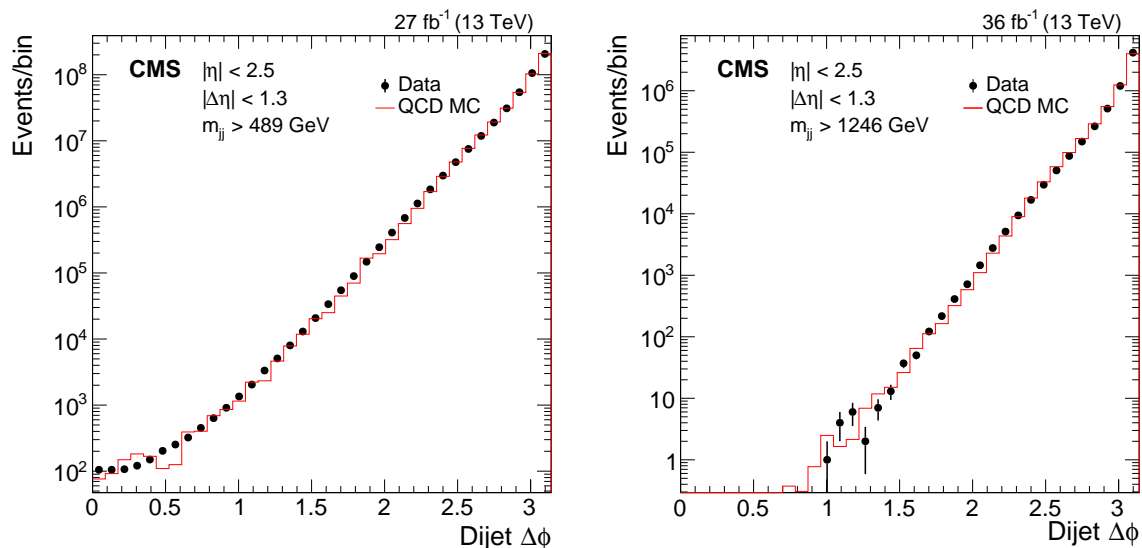


Figure 3: The azimuthal angular separation between the two wide jets (in radians) from the low-mass search (left) and the high-mass search (right). Data (points) are compared to QCD predictions from the PYTHIA 8 MC including detector simulation (histogram) normalized to the data.

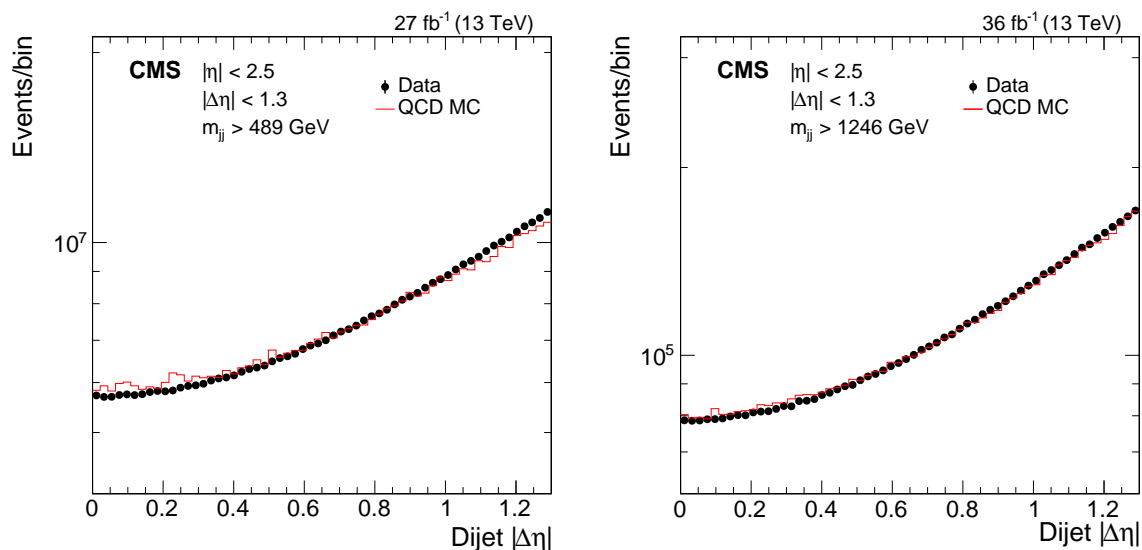


Figure 4: The pseudorapidity separation between the two wide jets from the low-mass search (left) and the high-mass search (right). Data (points) are compared to QCD predictions from the PYTHIA 8 MC including detector simulation (histogram) normalized to the data.

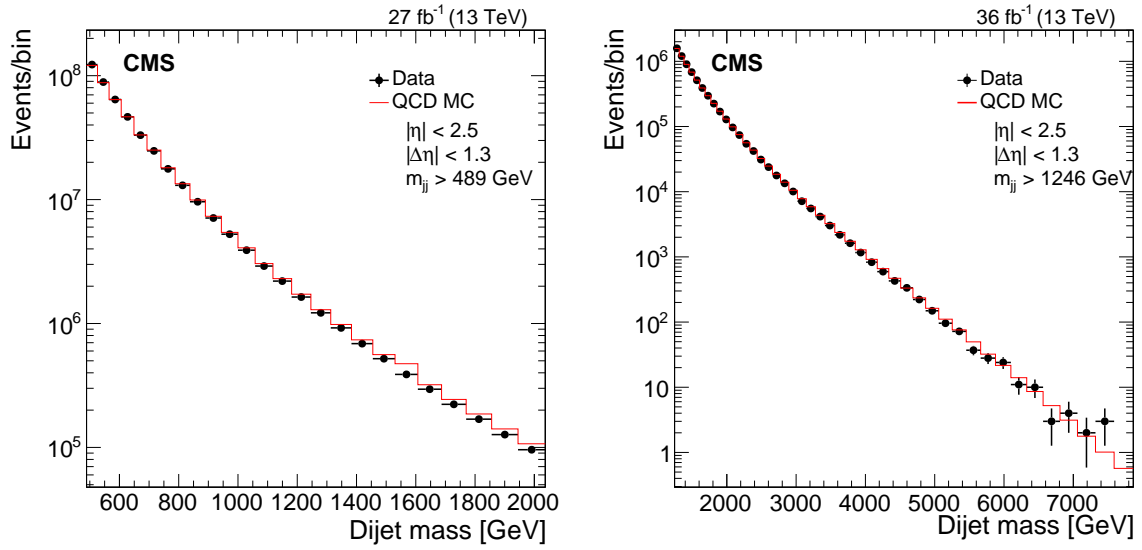


Figure 5: The dijet mass of the two wide jets from the low-mass search (left) and the high-mass search (right). Data (points) are compared to QCD predictions from the PYTHIA 8 MC including detector simulation (histogram) normalized to the data. The horizontal lines on the data points show the variable bin sizes.

However, the intrinsic uncertainties associated with QCD calculations make them unreliable estimators of the backgrounds in dijet resonance searches. Instead we will use the dijet data to estimate the background.

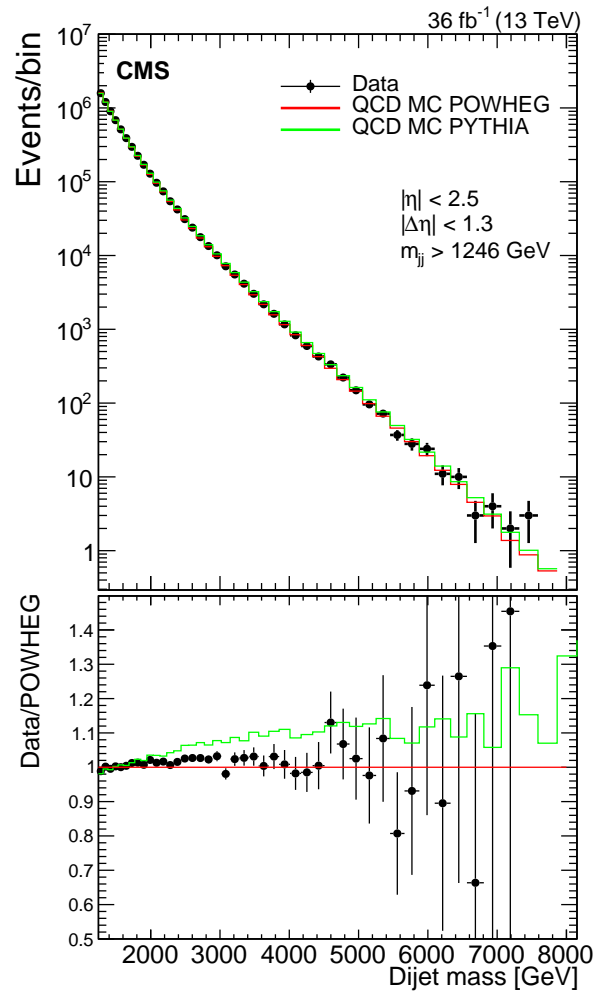


Figure 6: The dijet mass distribution of the two wide jets from the high-mass search. (Upper) Data (points) are compared to predictions from the POWHEG MC in red (darker) and the PYTHIA 8 MC in green (lighter), including detector simulation, each normalized to the data. (Lower) The ratio of data to the POWHEG prediction, compared to unity and compared to the ratio of the PYTHIA 8 MC to the POWHEG prediction. The horizontal lines on the data points show the variable bin sizes.

3 Search for narrow dijet resonances

3.1 Dijet mass spectra and background parameterizations

Figure 7 shows the dijet mass spectra, defined as the observed number of events in each bin divided by the integrated luminosity and the bin width, with bins of width corresponding to the dijet mass resolution. The bin edges and widths were chosen to be the same as those used by

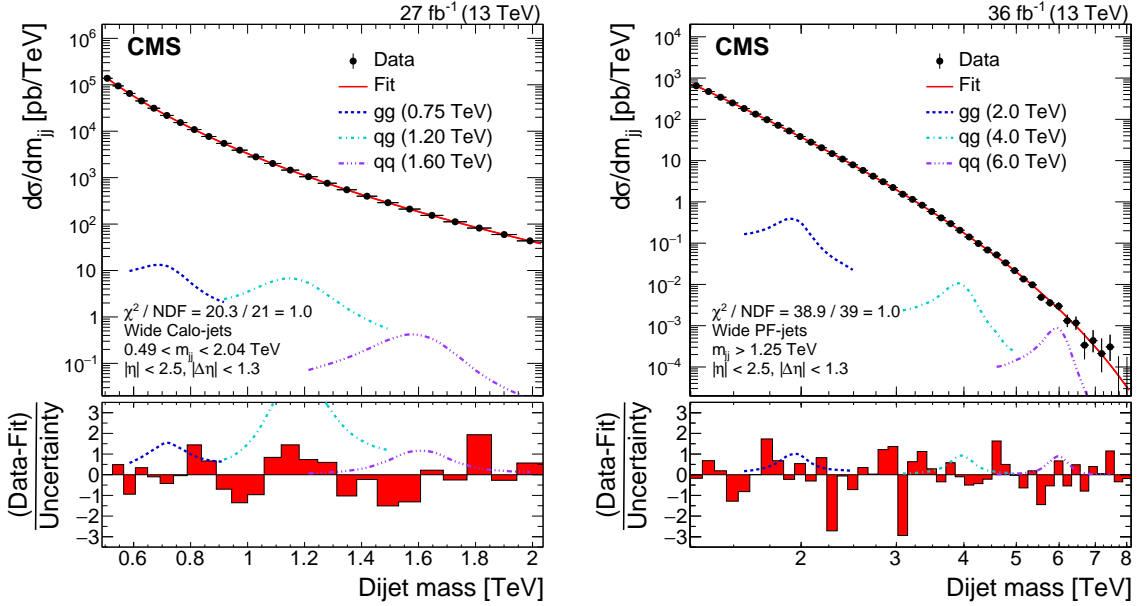


Figure 7: Dijet mass spectra (points) compared to a fitted parameterization of the background (solid curve) for the low-mass search (left) and the high-mass search (right). The horizontal lines on the data points show the variable bin sizes. The lower panel in each plot shows the difference between the data and the fitted parameterization, divided by the statistical uncertainty of the data. Examples of predicted signals from narrow gluon-gluon, quark-gluon, and quark-quark resonances are shown with cross sections equal to the observed upper limits at 95% CL.

previous dijet resonances searches performed by the CMS collaboration [4, 5, 7, 8, 10, 11, 14, 16]. The dijet mass spectrum for the high-mass search is fit with the parameterization

$$\frac{d\sigma}{dm_{jj}} = \frac{P_0(1-x)^{P_1}}{x^{P_2+P_3} \ln(x)}, \quad (1)$$

where $x = m_{jj}/\sqrt{s}$; and $P_0, P_1, P_2,$ and P_3 are four free fit parameters. The chi-squared per number of degrees of freedom of the fit is $\chi^2/NDF = 38.9/39$. The functional form in Eq. (1) was also used in previous searches [4–17, 51] to describe the data. For the low-mass search we used the following parameterization, which includes one additional parameter P_4 , to fit the dijet mass spectrum:

$$\frac{d\sigma}{dm_{jj}} = \frac{P_0(1-x)^{P_1}}{x^{P_2+P_3} \ln(x) + P_4 \ln^2(x)}. \quad (2)$$

Equation (2) with five parameters gives $\chi^2/NDF = 20.3/20$ when fit to the low-mass data, which is better than the $\chi^2/NDF = 27.9/21$ obtained using the four parameter functional form in Eq. (1). An F-test with a size $\alpha = 0.05$ [52] was used to confirm that no additional parameters

are needed to model these distributions, i.e. in the low-mass search including an additional term $P_5 \ln^3(x)$ in Eq.(2) gave $\chi^2/\text{NDF} = 20.1/19$, which corresponds to a smaller p -value than the fit with five parameters, and this six parameter functional form was found to be unnecessary by the Fisher F-test. The historical development of this family of parameterizations is discussed in Ref. [18]. The functional forms of Eqs. (1) and (2) are motivated by QCD calculations, where the term in the numerator behaves like the parton distribution functions at an average fractional momentum x of the two partons, and the term in the denominator gives a mass dependence similar to the QCD matrix elements. In Fig. 7, we show the result of the binned maximum likelihood fits, performed independently for the low-mass and high-mass searches. The dijet mass spectra are well modeled by the background fits. The lower panels of Fig. 7 show the pulls of the fit, which are the bin-by-bin differences between the data and the background fit divided by the statistical uncertainty of the data. In the overlap region of the dijet mass between 1.2 and 2.0 TeV, the pulls of the fit are not identical in the two searches because the fluctuations in reconstructed dijet mass for Calo-jets and PF-jets are not fully correlated.

3.2 Signal shapes, injection tests, and significance

Examples of dijet mass distributions for narrow resonances generated with the PYTHIA 8.205 program with the CUETP8M1 tune and including a GEANT4-based simulation of the CMS detector are shown in Fig. 7. The quark-quark (qq) resonances are modeled by $q\bar{q} \rightarrow G \rightarrow q\bar{q}$, the quark-gluon (qg) resonances are modeled by $qg \rightarrow q^* \rightarrow qg$, and the gluon-gluon (gg) resonances are modeled by $gg \rightarrow G \rightarrow gg$. The signal distributions shown in Fig. 7 are for qq, qg, and gg resonances with signal cross sections corresponding to the limits at 95% confidence level (CL) obtained by this analysis, as described below.

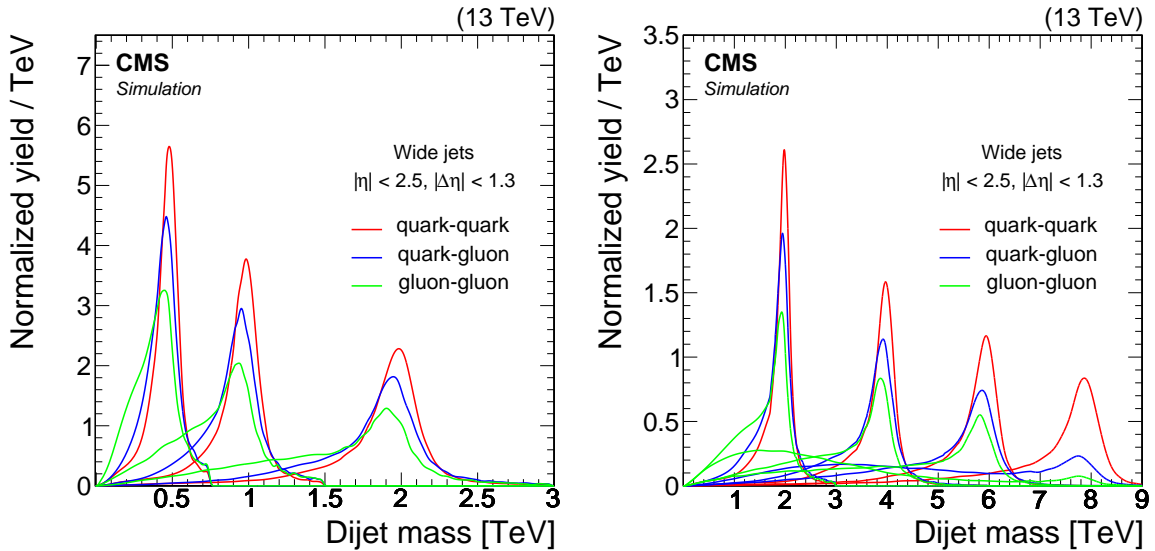


Figure 8: Signal shapes of narrow resonances with masses of 0.5, 1, and 2 TeV in the low-mass search (left) and masses of 2, 4, 6, and 8 TeV in the high-mass search (right). These reconstructed dijet mass spectra show wide jets from the PYTHIA 8 MC event generator including simulation of the CMS detector.

A more detailed view of the narrow-resonance signal shapes is provided in Fig. 8. The predicted mass distributions have Gaussian cores from jet energy resolution, and tails towards lower mass values primarily from QCD radiation. The observed width depends on the parton content of the resonance (qq, qg, or gg). The dijet mass resolution within the Gaussian core of gluon-gluon (quark-quark) resonances in Fig. 8 varies from 15(11)% at a resonance mass

of 0.5 TeV to 7.5 (6.3)% at 2 TeV for wide jets reconstructed using Calo-Jets, and varies from 6.2 (5.2)% at 2 TeV to 4.8 (4.0)% at 8 TeV for wide jets reconstructed using PF-Jets. The contribution of the low mass tail to the line shape also depends on the parton content of the resonance. Resonances decaying to gluons, which emit more QCD radiation than quarks, are broader and have a more pronounced tail. For the high-mass resonances, there is also a significant contribution that depends both on the parton distribution functions and on the natural width of the Breit–Wigner distribution. The low-mass component of the Breit–Wigner distribution of the resonance is amplified by the rise of the parton distribution function at low fractional momentum, as discussed in Section 7.3 of Ref. [53]. These effects cause a large tail at low mass values. Interference between the signal and the background processes is model dependent and not considered in this analysis. In some cases interference can modify the effective signal shape appreciably [54]. The signal shapes in the quark-quark channel come from quark-antiquark ($q\bar{q}$) resonances, which likely has a longer tail caused by parton distribution effects than that for diquark (qq) resonances, tending to make the quoted limits in the quark-quark channel conservative when applied to diquark signals.

Signal injection tests were performed to investigate the potential bias introduced through the choice of background parameterization. Two alternative parameterizations were found that model the dijet mass data using different functional forms:

$$\frac{d\sigma}{dm_{jj}} = P_0 \exp(P_1 x^{P_2} + P_3(1-x)^{P_4}) \quad (3)$$

and

$$\frac{d\sigma}{dm_{jj}} = \frac{P_0}{x^{P_1}} \exp(-P_2 x - P_3 x^2 - P_4 x^3). \quad (4)$$

Pseudo-data were generated, assuming a signal and these alternative parameterizations of the background, and then were fit with the nominal parameterization given in Eq. (2). The bias in the extracted signal was found to be negligible.

There is no evidence for a narrow resonance in the data. Using the statistical methodology discussed in Section 4.1, the local significance for qq , qg , and gg resonance signals was measured from 0.6 to 1.6 TeV in 50-GeV steps in the low-mass search, and from 1.6 to 8.1 TeV in 100-GeV steps in the high-mass search. The significance values obtained for qq resonances are shown in Fig. 9. The most significant excess of the data relative to the background fit comes from the two consecutive bins between 0.79 and 0.89 TeV. Fitting these data to qq , qg , and gg resonances with a mass of 0.85 TeV yields local significances of 1.2, 1.6, and 1.9 standard deviations, including systematic uncertainties, respectively.

4 Limits on narrow resonances

We use the dijet mass spectrum from wide jets, the background parameterization, and the dijet resonance shapes to set limits on the production cross section of new particles decaying to the parton pairs qq (or $q\bar{q}$), qg , and gg . A separate limit is determined for each final state because of the dependence of the dijet resonance shape on the types of the two final-state partons.

4.1 Systematic uncertainty and statistical methodology

The dominant sources of systematic uncertainty are the jet energy scale and resolution, integrated luminosity, and the value of the parameters within the functional form modeling the background shape in the dijet mass distribution. The uncertainty in the jet energy scale in both

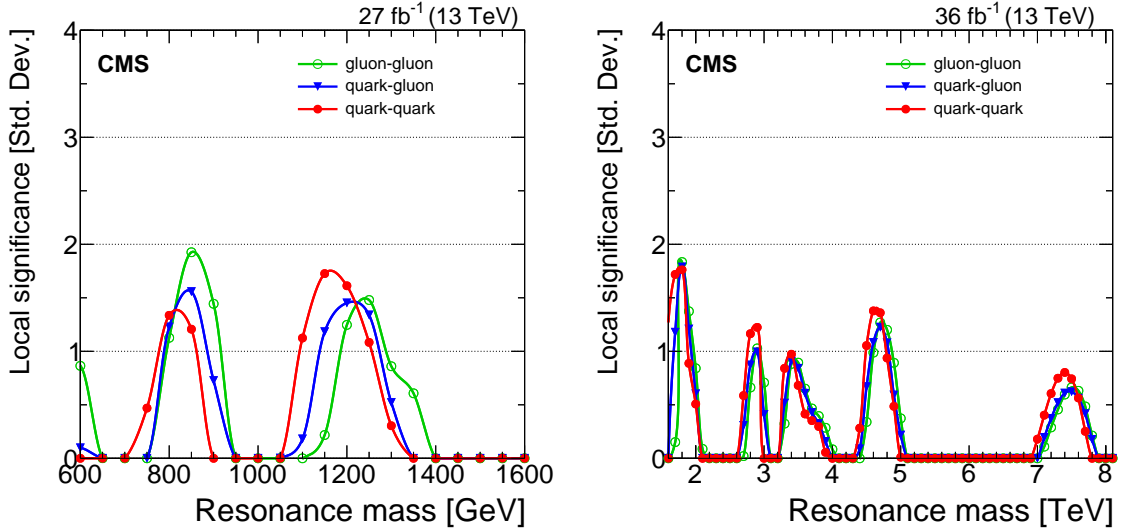


Figure 9: Local significance for a narrow resonance from the low-mass search (left) and the high-mass search (right).

the low-mass and the high-mass search is 2% and is determined from $\sqrt{s} = 13$ TeV data using the methods described in Ref. [40]. This uncertainty is propagated to the limits by shifting the dijet mass shape for signal by $\pm 2\%$. The uncertainty in the jet energy resolution translates into an uncertainty of 10% in the resolution of the dijet mass [40], and is propagated to the limits by observing the effect of increasing and decreasing by 10% the reconstructed width of the dijet mass shape for signal. The uncertainty in the integrated luminosity is 2.5% [55], and is propagated to the normalization of the signal. Changes in the values of the parameters describing the background introduce a change in the signal yield, which is accounted for as a systematic uncertainty as discussed in the next paragraph.

The asymptotic approximation [56] of the modified frequentist CL_s method [57, 58] is utilized to set upper limits on signal cross sections, following the prescription described in Ref. [59]. We use a multi-bin counting experiment likelihood, which is a product of Poisson distributions corresponding to different bins. We evaluate the likelihood independently at each value of the resonance pole mass from 0.6 to 1.6 TeV in 50-GeV steps in the low-mass search, and from 1.6 to 8.1 TeV in 100-GeV steps in the high-mass search. The contribution from each hypothetical resonance signal is evaluated in every bin of dijet mass greater than the minimum dijet mass requirement in the search and less than 150% of the resonance mass (e.g. the high mass tail of a 1 TeV resonance is truncated, removing any contribution above a dijet mass of 1.5 TeV, but the low mass tail is not truncated). The systematic uncertainties are implemented as nuisance parameters in the likelihood model, with Gaussian constraints for the jet energy scale and resolution, and log-normal constraints for the integrated luminosity. The systematic uncertainty in the background is automatically evaluated via profiling, effectively refitting for the optimal values of the background parameters for each value of resonance cross section. The extent to which the background uncertainty affects the limit depends significantly on the signal shape and the resonance mass, with the largest effect occurring for the gg resonances, because they are broader, and the smallest effect for qq resonances. The effect decreases as the resonance mass increases. The effect of the systematic uncertainties on the limit for qq resonances is shown in Fig. 10. For almost all resonance mass values, the background systematic uncertainty produces the majority of the effect on the limit shown here.

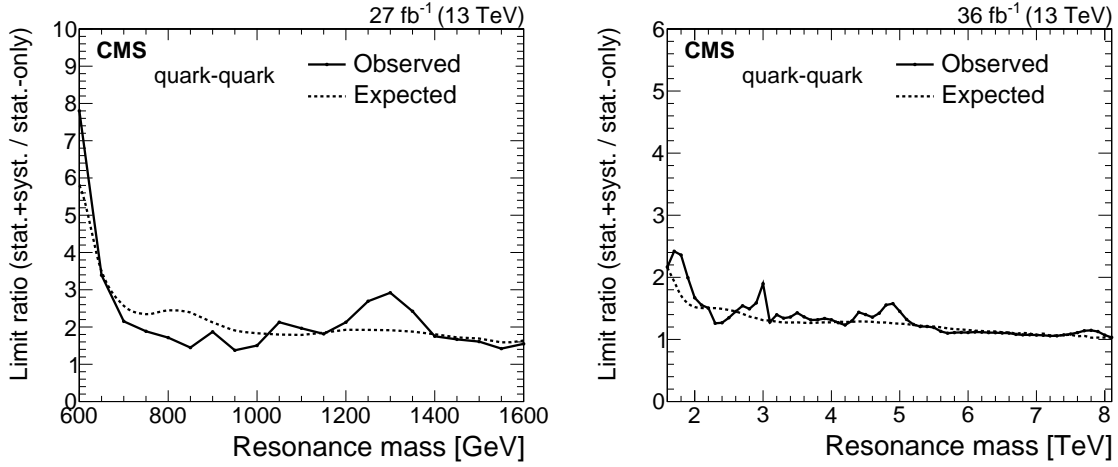


Figure 10: The observed (points) and expected (dashed) ratio between the 95% CL limit on the cross section, including systematic uncertainties, and the limit including statistical uncertainties only for dijet resonances decaying to quark-quark in the low-mass search (left) and in the high-mass search (right).

4.2 Limits on the resonance production cross section

Tables 1 and 2, and Figs. 11 and 12, show the model-independent observed upper limits at 95% CL on the product of the cross section (σ), the branching fraction to dijets (B), and the acceptance (A) for narrow resonances, with the kinematic requirements $|\Delta\eta| < 1.3$ for the dijet system and $|\eta| < 2.5$ for each of the jets. The acceptance of the minimum dijet mass requirement in each search has been evaluated separately for qq, qg, and gg resonances, and has been taken into account by correcting the limits and therefore does not appear in the acceptance A . The resonance mass boundary of 1.6 TeV between the high- and low-mass searches was chosen to maintain a reasonable acceptance for the minimum dijet mass requirement imposed by the high-mass search. For a 1.6 TeV dijet resonance, the acceptance of the 1.25 TeV dijet mass requirement is 57% for a gluon-gluon resonance, 76% for a quark-gluon resonance, and 85% for a quark-quark resonance. At this resonance mass, the expected limits we find on σBA for a quark-quark resonance are the same in the high and low mass search. Figure 11 also shows the expected limits on σBA and their bands of uncertainty. The difference in the limits for qq, qg, and gg resonances at the same resonance mass originates from the difference in their line shapes. For the RS graviton model, which decays to both $q\bar{q}$ and gg final states, the upper limits on the cross section are derived using a weighted average of the qq and gg resonance shapes, where the weights correspond to the relative branching fractions for the two final states.

Table 1: Limits from the low-mass search. The observed and expected upper limits at 95% CL on σBA for gluon-gluon, quark-gluon, and quark-quark resonances, and an RS graviton are given as a function of the resonance mass.

Mass [TeV]	95% CL upper limit [pb]							
	gg		qg		qq		RS graviton	
	Observed	Expected	Observed	Expected	Observed	Expected	Observed	Expected
0.60	$3.93 \times 10^{+1}$	$2.10 \times 10^{+1}$	$3.37 \times 10^{+1}$	$1.90 \times 10^{+1}$	$1.38 \times 10^{+1}$	$1.05 \times 10^{+1}$	$2.59 \times 10^{+1}$	$1.46 \times 10^{+1}$
0.65	$1.55 \times 10^{+1}$	$1.77 \times 10^{+1}$	$1.01 \times 10^{+1}$	$1.14 \times 10^{+1}$	4.92×10^0	5.15×10^0	6.92×10^0	8.28×10^0
0.70	6.14×10^0	$1.12 \times 10^{+1}$	4.73×10^0	6.32×10^0	2.47×10^0	3.16×10^0	3.59×10^0	4.77×10^0
0.75	5.50×10^0	8.13×10^0	3.82×10^0	4.68×10^0	2.64×10^0	2.49×10^0	3.57×10^0	3.67×10^0
0.80	$1.02 \times 10^{+1}$	7.15×10^0	5.73×10^0	4.06×10^0	3.14×10^0	2.14×10^0	4.39×10^0	3.11×10^0
0.85	$1.13 \times 10^{+1}$	5.93×10^0	5.45×10^0	3.33×10^0	2.46×10^0	1.79×10^0	4.35×10^0	2.55×10^0
0.90	7.56×10^0	4.04×10^0	3.21×10^0	2.42×10^0	1.17×10^0	1.36×10^0	2.45×10^0	2.04×10^0
0.95	3.23×10^0	3.32×10^0	1.40×10^0	1.86×10^0	7.30×10^{-1}	1.10×10^0	1.01×10^0	1.59×10^0
1.00	1.66×10^0	2.60×10^0	9.67×10^{-1}	1.45×10^0	5.72×10^{-1}	9.06×10^{-1}	8.19×10^{-1}	1.23×10^0
1.05	1.41×10^0	2.22×10^0	1.11×10^0	1.26×10^0	9.11×10^{-1}	7.90×10^{-1}	1.14×10^0	1.11×10^0
1.10	2.06×10^0	1.96×10^0	1.90×10^0	1.13×10^0	1.51×10^0	7.11×10^{-1}	1.90×10^0	9.86×10^{-1}
1.15	3.90×10^0	1.79×10^0	2.58×10^0	1.04×10^0	1.74×10^0	6.55×10^{-1}	1.87×10^0	9.12×10^{-1}
1.20	4.49×10^0	1.63×10^0	2.74×10^0	9.49×10^{-1}	1.38×10^0	6.00×10^{-1}	1.91×10^0	8.39×10^{-1}
1.25	3.48×10^0	1.45×10^0	2.04×10^0	8.64×10^{-1}	1.23×10^0	5.40×10^{-1}	1.96×10^0	7.72×10^{-1}
1.30	3.58×10^0	1.26×10^0	2.00×10^0	7.60×10^{-1}	8.61×10^{-1}	4.85×10^{-1}	1.48×10^0	6.87×10^{-1}
1.35	1.96×10^0	1.11×10^0	1.01×10^0	6.62×10^{-1}	4.85×10^{-1}	4.24×10^{-1}	9.35×10^{-1}	6.01×10^{-1}
1.40	1.14×10^0	9.55×10^{-1}	5.56×10^{-1}	5.71×10^{-1}	3.00×10^{-1}	3.69×10^{-1}	4.47×10^{-1}	5.16×10^{-1}
1.45	6.32×10^{-1}	8.33×10^{-1}	3.52×10^{-1}	4.97×10^{-1}	1.86×10^{-1}	3.27×10^{-1}	2.75×10^{-1}	4.55×10^{-1}
1.50	4.20×10^{-1}	7.23×10^{-1}	2.66×10^{-1}	4.30×10^{-1}	1.45×10^{-1}	2.84×10^{-1}	2.29×10^{-1}	4.00×10^{-1}
1.55	3.57×10^{-1}	6.38×10^{-1}	1.93×10^{-1}	3.81×10^{-1}	1.44×10^{-1}	2.59×10^{-1}	1.97×10^{-1}	3.57×10^{-1}
1.60	3.37×10^{-1}	5.58×10^{-1}	1.87×10^{-1}	3.45×10^{-1}	1.64×10^{-1}	2.35×10^{-1}	2.01×10^{-1}	3.20×10^{-1}

Table 2: Limits from the high-mass search. The observed and expected upper limits at 95% CL on σBA for gluon-gluon, quark-gluon, and quark-quark resonances, and an RS graviton are shown as functions of the resonance mass.

Mass [TeV]	95% CL upper limit [pb]							
	gg		qg		qq		RS graviton	
	Observed	Expected	Observed	Expected	Observed	Expected	Observed	Expected
1.6	3.72×10^{-1}	6.72×10^{-1}	2.74×10^{-1}	4.08×10^{-1}	2.07×10^{-1}	2.38×10^{-1}	2.65×10^{-1}	3.46×10^{-1}
1.7	6.50×10^{-1}	5.02×10^{-1}	4.33×10^{-1}	2.96×10^{-1}	2.99×10^{-1}	1.79×10^{-1}	4.06×10^{-1}	2.61×10^{-1}
1.8	6.17×10^{-1}	3.55×10^{-1}	3.86×10^{-1}	2.10×10^{-1}	2.62×10^{-1}	1.34×10^{-1}	3.66×10^{-1}	1.92×10^{-1}
1.9	4.71×10^{-1}	2.63×10^{-1}	2.69×10^{-1}	1.60×10^{-1}	1.61×10^{-1}	1.06×10^{-1}	2.46×10^{-1}	1.48×10^{-1}
2.0	2.97×10^{-1}	2.07×10^{-1}	1.67×10^{-1}	1.29×10^{-1}	1.08×10^{-1}	8.71×10^{-2}	1.59×10^{-1}	1.22×10^{-1}
2.1	1.88×10^{-1}	1.74×10^{-1}	1.12×10^{-1}	1.10×10^{-1}	7.56×10^{-2}	7.44×10^{-2}	1.08×10^{-1}	1.03×10^{-1}
2.2	1.34×10^{-1}	1.50×10^{-1}	7.53×10^{-2}	9.49×10^{-2}	4.90×10^{-2}	6.43×10^{-2}	7.18×10^{-2}	8.95×10^{-2}
2.3	8.15×10^{-2}	1.30×10^{-1}	4.62×10^{-2}	8.32×10^{-2}	2.86×10^{-2}	5.57×10^{-2}	4.19×10^{-2}	7.78×10^{-2}
2.4	5.89×10^{-2}	1.13×10^{-1}	3.84×10^{-2}	7.21×10^{-2}	2.80×10^{-2}	4.82×10^{-2}	3.75×10^{-2}	6.78×10^{-2}
2.5	5.96×10^{-2}	9.73×10^{-2}	4.15×10^{-2}	6.23×10^{-2}	3.05×10^{-2}	4.16×10^{-2}	4.04×10^{-2}	5.86×10^{-2}
2.6	6.67×10^{-2}	8.32×10^{-2}	4.71×10^{-2}	5.33×10^{-2}	3.47×10^{-2}	3.58×10^{-2}	4.61×10^{-2}	5.05×10^{-2}
2.7	7.32×10^{-2}	7.09×10^{-2}	5.22×10^{-2}	4.55×10^{-2}	3.88×10^{-2}	3.08×10^{-2}	5.19×10^{-2}	4.33×10^{-2}
2.8	7.79×10^{-2}	6.04×10^{-2}	5.26×10^{-2}	3.91×10^{-2}	3.87×10^{-2}	2.63×10^{-2}	5.27×10^{-2}	3.70×10^{-2}
2.9	7.37×10^{-2}	5.18×10^{-2}	4.82×10^{-2}	3.35×10^{-2}	3.53×10^{-2}	2.28×10^{-2}	4.82×10^{-2}	3.20×10^{-2}
3.0	6.42×10^{-2}	4.43×10^{-2}	3.96×10^{-2}	2.90×10^{-2}	2.68×10^{-2}	1.96×10^{-2}	3.89×10^{-2}	2.77×10^{-2}
3.1	4.20×10^{-2}	3.86×10^{-2}	2.46×10^{-2}	2.53×10^{-2}	1.36×10^{-2}	1.74×10^{-2}	2.08×10^{-2}	2.43×10^{-2}
3.2	2.95×10^{-2}	3.37×10^{-2}	2.11×10^{-2}	2.24×10^{-2}	1.64×10^{-2}	1.54×10^{-2}	2.15×10^{-2}	2.16×10^{-2}
3.3	3.41×10^{-2}	2.96×10^{-2}	2.36×10^{-2}	1.96×10^{-2}	1.78×10^{-2}	1.36×10^{-2}	2.39×10^{-2}	1.91×10^{-2}
3.4	3.47×10^{-2}	2.63×10^{-2}	2.34×10^{-2}	1.75×10^{-2}	1.69×10^{-2}	1.22×10^{-2}	2.32×10^{-2}	1.70×10^{-2}
3.5	3.19×10^{-2}	2.33×10^{-2}	2.14×10^{-2}	1.58×10^{-2}	1.48×10^{-2}	1.10×10^{-2}	2.06×10^{-2}	1.53×10^{-2}
3.6	2.74×10^{-2}	2.08×10^{-2}	1.82×10^{-2}	1.41×10^{-2}	1.19×10^{-2}	9.81×10^{-3}	1.70×10^{-2}	1.37×10^{-2}
3.7	2.25×10^{-2}	1.87×10^{-2}	1.52×10^{-2}	1.27×10^{-2}	1.01×10^{-2}	8.86×10^{-3}	1.44×10^{-2}	1.24×10^{-2}
3.8	1.96×10^{-2}	1.68×10^{-2}	1.31×10^{-2}	1.16×10^{-2}	9.02×10^{-3}	8.03×10^{-3}	1.27×10^{-2}	1.12×10^{-2}
3.9	1.72×10^{-2}	1.53×10^{-2}	1.13×10^{-2}	1.05×10^{-2}	7.72×10^{-3}	7.25×10^{-3}	1.09×10^{-2}	1.01×10^{-2}
4.0	1.47×10^{-2}	1.37×10^{-2}	9.57×10^{-3}	9.45×10^{-3}	6.29×10^{-3}	6.57×10^{-3}	9.04×10^{-3}	9.16×10^{-3}
4.1	1.21×10^{-2}	1.25×10^{-2}	8.06×10^{-3}	8.67×10^{-3}	5.17×10^{-3}	5.98×10^{-3}	7.46×10^{-3}	8.33×10^{-3}
4.2	1.02×10^{-2}	1.14×10^{-2}	6.93×10^{-3}	7.89×10^{-3}	4.52×10^{-3}	5.40×10^{-3}	6.45×10^{-3}	7.59×10^{-3}
4.3	9.12×10^{-3}	1.03×10^{-2}	6.55×10^{-3}	7.20×10^{-3}	4.61×10^{-3}	4.91×10^{-3}	6.29×10^{-3}	6.86×10^{-3}
4.4	9.27×10^{-3}	9.35×10^{-3}	7.01×10^{-3}	6.57×10^{-3}	5.35×10^{-3}	4.46×10^{-3}	7.02×10^{-3}	6.23×10^{-3}
4.5	1.02×10^{-2}	8.47×10^{-3}	7.52×10^{-3}	5.98×10^{-3}	5.65×10^{-3}	4.04×10^{-3}	7.60×10^{-3}	5.64×10^{-3}
4.6	1.05×10^{-2}	7.69×10^{-3}	7.51×10^{-3}	5.44×10^{-3}	5.55×10^{-3}	3.65×10^{-3}	7.54×10^{-3}	5.10×10^{-3}
4.7	1.03×10^{-2}	6.96×10^{-3}	7.27×10^{-3}	4.91×10^{-3}	5.26×10^{-3}	3.31×10^{-3}	7.16×10^{-3}	4.63×10^{-3}
4.8	9.62×10^{-3}	6.27×10^{-3}	6.72×10^{-3}	4.46×10^{-3}	4.79×10^{-3}	2.99×10^{-3}	6.51×10^{-3}	4.19×10^{-3}
4.9	8.56×10^{-3}	5.69×10^{-3}	5.86×10^{-3}	4.04×10^{-3}	3.88×10^{-3}	2.70×10^{-3}	5.44×10^{-3}	3.77×10^{-3}
5.0	6.90×10^{-3}	5.10×10^{-3}	4.62×10^{-3}	3.67×10^{-3}	2.85×10^{-3}	2.44×10^{-3}	4.12×10^{-3}	3.41×10^{-3}
5.1	5.34×10^{-3}	4.70×10^{-3}	3.53×10^{-3}	3.33×10^{-3}	2.14×10^{-3}	2.22×10^{-3}	3.12×10^{-3}	3.11×10^{-3}
5.2	4.11×10^{-3}	4.28×10^{-3}	2.77×10^{-3}	3.04×10^{-3}	1.73×10^{-3}	2.01×10^{-3}	2.50×10^{-3}	2.82×10^{-3}
5.3	3.35×10^{-3}	3.94×10^{-3}	2.28×10^{-3}	2.77×10^{-3}	1.45×10^{-3}	1.81×10^{-3}	2.09×10^{-3}	2.58×10^{-3}
5.4	2.85×10^{-3}	3.60×10^{-3}	1.92×10^{-3}	2.50×10^{-3}	1.22×10^{-3}	1.64×10^{-3}	1.76×10^{-3}	2.34×10^{-3}
5.5	2.43×10^{-3}	3.28×10^{-3}	1.62×10^{-3}	2.29×10^{-3}	1.01×10^{-3}	1.50×10^{-3}	1.47×10^{-3}	2.13×10^{-3}
5.6	2.05×10^{-3}	3.02×10^{-3}	1.38×10^{-3}	2.08×10^{-3}	8.54×10^{-4}	1.36×10^{-3}	1.25×10^{-3}	1.93×10^{-3}
5.7	1.78×10^{-3}	2.77×10^{-3}	1.22×10^{-3}	1.90×10^{-3}	7.88×10^{-4}	1.23×10^{-3}	1.13×10^{-3}	1.76×10^{-3}
5.8	1.65×10^{-3}	2.53×10^{-3}	1.15×10^{-3}	1.73×10^{-3}	8.00×10^{-4}	1.11×10^{-3}	1.12×10^{-3}	1.61×10^{-3}
5.9	1.64×10^{-3}	2.33×10^{-3}	1.14×10^{-3}	1.58×10^{-3}	8.09×10^{-4}	1.02×10^{-3}	1.13×10^{-3}	1.47×10^{-3}
6.0	1.64×10^{-3}	2.13×10^{-3}	1.13×10^{-3}	1.43×10^{-3}	7.91×10^{-4}	9.25×10^{-4}	1.11×10^{-3}	1.34×10^{-3}
6.1	1.66×10^{-3}	2.01×10^{-3}	1.11×10^{-3}	1.34×10^{-3}	7.45×10^{-4}	8.39×10^{-4}	1.07×10^{-3}	1.24×10^{-3}
6.2	1.63×10^{-3}	1.89×10^{-3}	1.06×10^{-3}	1.24×10^{-3}	6.84×10^{-4}	7.66×10^{-4}	1.01×10^{-3}	1.14×10^{-3}
6.3	1.56×10^{-3}	1.79×10^{-3}	1.00×10^{-3}	1.16×10^{-3}	6.26×10^{-4}	6.99×10^{-4}	9.36×10^{-4}	1.05×10^{-3}
6.4	1.49×10^{-3}	1.69×10^{-3}	9.41×10^{-4}	1.08×10^{-3}	5.75×10^{-4}	6.44×10^{-4}	8.66×10^{-4}	9.74×10^{-4}
6.5	1.42×10^{-3}	1.61×10^{-3}	8.82×10^{-4}	1.00×10^{-3}	5.21×10^{-4}	5.89×10^{-4}	8.00×10^{-4}	9.00×10^{-4}
6.6	1.36×10^{-3}	1.53×10^{-3}	8.26×10^{-4}	9.37×10^{-4}	4.72×10^{-4}	5.40×10^{-4}	7.33×10^{-4}	8.39×10^{-4}
6.7	1.29×10^{-3}	1.47×10^{-3}	7.79×10^{-4}	8.82×10^{-4}	4.30×10^{-4}	4.91×10^{-4}	6.81×10^{-4}	7.78×10^{-4}
6.8	1.24×10^{-3}	1.41×10^{-3}	7.35×10^{-4}	8.27×10^{-4}	4.06×10^{-4}	4.55×10^{-4}	6.46×10^{-4}	7.23×10^{-4}
6.9	1.21×10^{-3}	1.36×10^{-3}	7.11×10^{-4}	7.78×10^{-4}	4.00×10^{-4}	4.18×10^{-4}	6.38×10^{-4}	6.74×10^{-4}
7.0	1.24×10^{-3}	1.32×10^{-3}	7.08×10^{-4}	7.29×10^{-4}	3.98×10^{-4}	3.81×10^{-4}	6.44×10^{-4}	6.32×10^{-4}
7.1	1.31×10^{-3}	1.30×10^{-3}	7.27×10^{-4}	7.05×10^{-4}	3.94×10^{-4}	3.57×10^{-4}	6.52×10^{-4}	5.89×10^{-4}
7.2	1.38×10^{-3}	1.30×10^{-3}	7.40×10^{-4}	6.81×10^{-4}	3.86×10^{-4}	3.27×10^{-4}	6.50×10^{-4}	5.58×10^{-4}
7.3	1.46×10^{-3}	1.30×10^{-3}	7.53×10^{-4}	6.62×10^{-4}	3.74×10^{-4}	3.02×10^{-4}	6.39×10^{-4}	5.28×10^{-4}
7.4	1.54×10^{-3}	1.32×10^{-3}	7.61×10^{-4}	6.50×10^{-4}	3.57×10^{-4}	2.84×10^{-4}	6.22×10^{-4}	4.97×10^{-4}
7.5	1.62×10^{-3}	1.36×10^{-3}	7.62×10^{-4}	6.38×10^{-4}	3.33×10^{-4}	2.66×10^{-4}	5.91×10^{-4}	4.73×10^{-4}
7.6	1.71×10^{-3}	1.42×10^{-3}	7.59×10^{-4}	6.38×10^{-4}	3.10×10^{-4}	2.47×10^{-4}	5.55×10^{-4}	4.55×10^{-4}
7.7	1.81×10^{-3}	1.51×10^{-3}	7.53×10^{-4}	6.38×10^{-4}	2.84×10^{-4}	2.29×10^{-4}	5.15×10^{-4}	4.36×10^{-4}
7.8	1.93×10^{-3}	1.65×10^{-3}	7.43×10^{-4}	6.44×10^{-4}	2.50×10^{-4}	2.17×10^{-4}	4.65×10^{-4}	4.18×10^{-4}
7.9	2.06×10^{-3}	1.87×10^{-3}	7.19×10^{-4}	6.56×10^{-4}	2.20×10^{-4}	2.11×10^{-4}	4.20×10^{-4}	4.18×10^{-4}
8.0	2.25×10^{-3}	2.24×10^{-3}	7.03×10^{-4}	6.93×10^{-4}	1.99×10^{-4}	2.11×10^{-4}	3.98×10^{-4}	4.24×10^{-4}
8.1	2.26×10^{-3}	2.41×10^{-3}	7.05×10^{-4}	7.35×10^{-4}	1.97×10^{-4}	2.17×10^{-4}	4.05×10^{-4}	4.55×10^{-4}

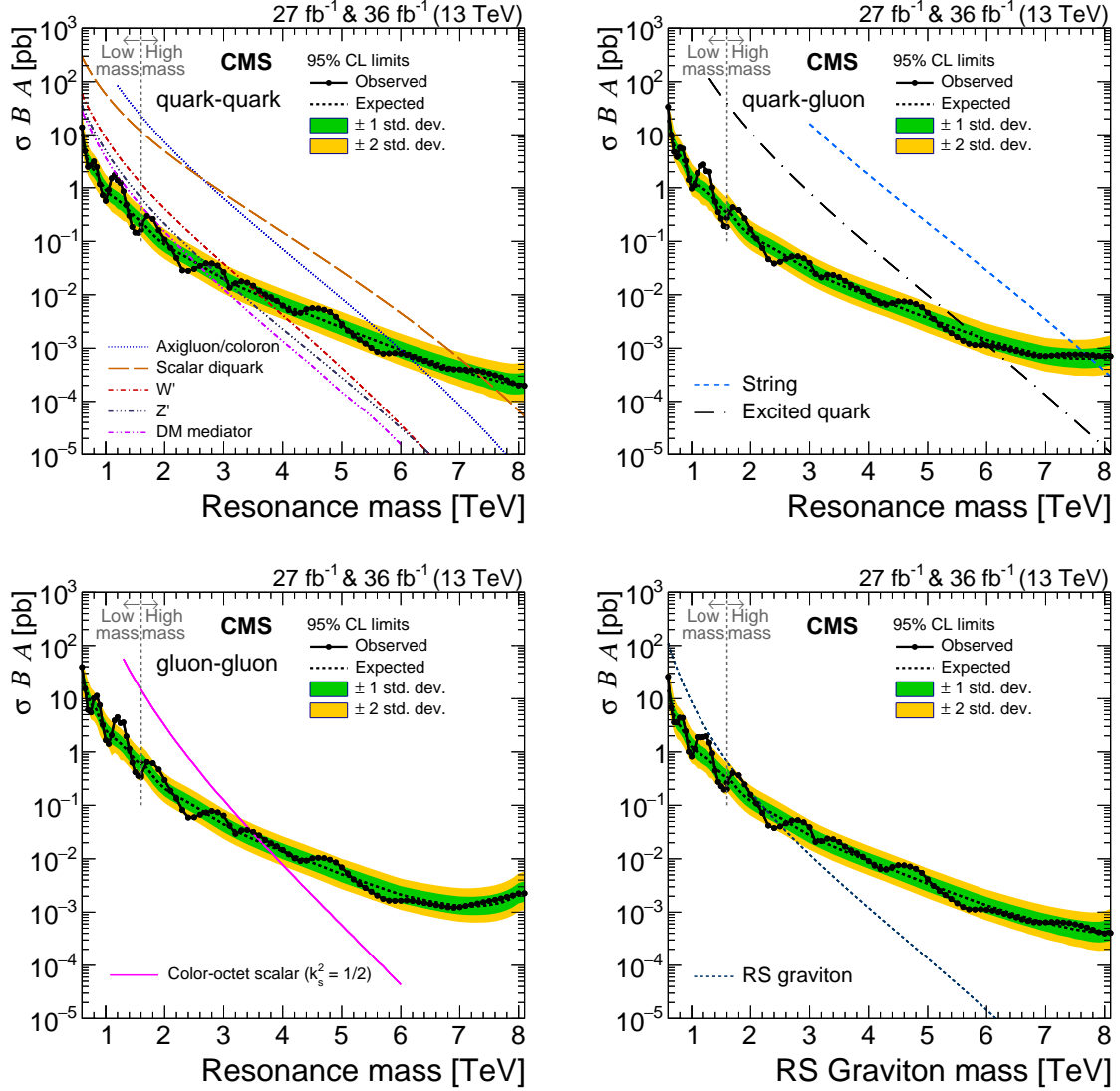


Figure 11: The observed 95% CL upper limits on the product of the cross section, branching fraction, and acceptance for dijet resonances decaying to quark-quark (upper left), quark-gluon (upper right), gluon-gluon (lower left), and for RS gravitons (lower right). The corresponding expected limits (dashed) and their variations at the 1 and 2 standard deviation levels (shaded bands) are also shown. Limits are compared to predicted cross sections for string resonances [20, 21], excited quarks [23, 24], axigluons [25], colorons [26], scalar diquarks [22], color-octet scalars [27], new gauge bosons W' and Z' with SM-like couplings [29], dark matter mediators for $m_{\text{DM}} = 1 \text{ GeV}$ [31, 32], and RS gravitons [30].

4.3 Limits on the resonance mass for benchmark models

All upper limits presented can be compared to the parton-level predictions of σBA , without detector simulation, to determine mass limits on new particles. The model predictions shown in Figs. 11 and 12 are calculated in the narrow-width approximation [18] using the CTEQ6L1 [60] parton distribution functions at leading order. A next-to-leading order correction factor of $K = 1 + 8\pi\alpha_S/9 \approx 1.3$ is applied to the leading order predictions for the W' model and $K = 1 + (4\alpha_S/6\pi)(1 + 4\pi^2/3) \approx 1.3$ for the Z' model (see pages 248 and 233 of Ref. [61]), where α_S is the strong coupling constant evaluated at a renormalization scale equal to the res-

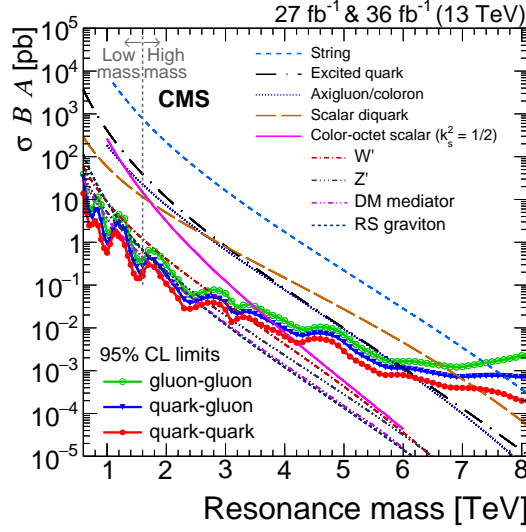


Figure 12: The observed 95% CL upper limits on the product of the cross section, branching fraction, and acceptance for quark-quark, quark-gluon, and gluon-gluon dijet resonances. Limits are compared to predicted cross sections for string resonances [20, 21], excited quarks [23, 24], axigluons [25], colorons [26], scalar diquarks [22], color-octet scalars [27], new gauge bosons W' and Z' with SM-like couplings [29], dark matter mediators for $m_{\text{DM}} = 1$ GeV [31, 32], and RS gravitons [30].

onance mass. Similarly, for the axigluon/coloron models a correction factor is applied which varies between $K = 1.08$ at a resonance mass of 0.6 TeV and $K = 1.33$ at 8.1 TeV [62]. The branching fraction includes the direct decays of the resonance into the five light quarks and gluons only, excluding top quarks from the decay, although top quarks are included in the calculation of the resonance width. The signal acceptance evaluated at the parton level for the resonance decay to two partons can be written as $A = A_{\Delta} A_{\eta}$, where A_{Δ} is the acceptance of requiring $|\Delta\eta| < 1.3$ alone, and A_{η} is the acceptance of also requiring $|\eta| < 2.5$. The acceptance A_{Δ} is model dependent. In the case of isotropic decays, the dijet angular distribution as a function of $\tanh(|\Delta\eta|/2)$ is approximately constant, and $A_{\Delta} \approx \tanh(1.3/2) = 0.57$, independent of resonance mass. The acceptance A_{η} is maximal for resonance masses above 1 TeV—greater than 0.99 for all models considered. The acceptance A_{η} decreases as the resonance mass decreases below 1 TeV, and for a resonance mass of 0.6 TeV it is 0.92 for excited quarks, 0.98 for RS gravitons, and between those two values for the other models. For a given model, new particles are excluded at 95% CL in mass regions where the theoretical prediction lies at or above the observed upper limit for the appropriate final state of Figs. 11 and 12. Mass limits on all benchmark models are summarized in Table 3.

Table 3: Observed and expected mass limits at 95% CL from this analysis compared to previously published limits on narrow resonances from CMS with 12.9 fb^{-1} [4]. The listed models are excluded between 0.6 TeV and the indicated mass limit by this analysis. In addition to the observed mass limits listed below, this analysis also excludes the RS graviton model within the mass interval between 1.9 and 2.5 TeV and the Z' model within roughly a 50 GeV window around 3.1 TeV.

Model	Final State	Observed (expected) mass limit [TeV]	
		36 fb^{-1}	Ref. [4], 12.9 fb^{-1}
String resonance	qg	7.7 (7.7)	7.4 (7.4)
Scalar diquark	qq	7.2 (7.4)	6.9 (6.8)
Axigluon/coloron	q \bar{q}	6.1 (6.0)	5.5 (5.6)
Excited quark	qg	6.0 (5.8)	5.4 (5.4)
Color-octet scalar ($k_s^2 = 1/2$)	gg	3.4 (3.6)	3.0 (3.3)
W' SM-like	q \bar{q}	3.3 (3.6)	2.7 (3.1)
Z' SM-like	q \bar{q}	2.7 (2.9)	2.1 (2.3)
RS graviton ($k/\overline{M}_{\text{Pl}} = 0.1$)	q \bar{q} , gg	1.8 (2.3)	1.9 (1.8)
DM mediator ($m_{\text{DM}} = 1 \text{ GeV}$)	q \bar{q}	2.6 (2.5)	2.0 (2.0)

4.4 Limits on the coupling to quarks of a leptophobic Z'

Mass limits on new particles are sensitive to the assumptions about their coupling. Furthermore, at a fixed resonance mass, as the search sensitivity increases we can exclude models with smaller couplings. Figure 13 shows upper limits on the coupling as a function of mass for a leptophobic Z' resonance which has a natural width

$$\Gamma = \frac{3(g'_q)^2 M}{2\pi} \quad (5)$$

where M is the resonance mass. Limits are only shown in Fig. 13 for coupling values $g'_q < 0.45$, corresponding to a width less than 10% of the resonance mass, for which our narrow resonance limits are approximately valid. To constrain larger values of the coupling we will consider broad resonances in Section 6.

5 Limits on a dark matter mediator

We use our limits to constrain simplified models of DM, with leptophobic vector and axial-vector mediators that couple only to quarks and DM particles [31, 32]. Figure 14 shows the excluded values of mediator mass as a function of m_{DM} , for both types of mediators. For $m_{\text{DM}} = 1 \text{ GeV}$ the observed excluded range of the mediator mass (M_{Med}) is between 0.6 and 2.6 TeV, as also shown in Fig. 11 and listed in Table 3. The limits on a dark matter mediator are indistinguishable for $m_{\text{DM}} = 0$ and 1 GeV. In Fig. 14 the expected upper value of excluded M_{Med} increases with m_{DM} because the branching fraction to $q\bar{q}$ increases with m_{DM} . In Fig. 14 our exclusions are compared to constraints from the cosmological relic density of DM determined from astrophysical measurements [63, 64] and from MADDM version 2.0.6 [65, 66] as described in Ref. [67].

5.1 Relationship of the DM mediator model to the leptophobic Z' model

If $m_{\text{DM}} > M_{\text{Med}}/2$, the mediator cannot decay to DM particles, and the dijet cross section from the mediator models [31] becomes identical to that in the leptophobic Z' model [33] used in

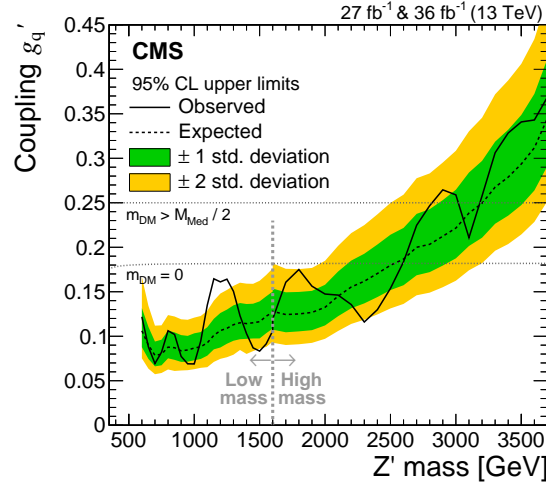


Figure 13: The 95% CL upper limits on the universal quark coupling g'_q as a function of resonance mass for a leptophobic Z' resonance that only couples to quarks. The observed limits (solid), expected limits (dashed) and their variation at the 1 and 2 standard deviation levels (shaded bands) are shown. The dotted horizontal lines show the coupling strength for which the cross section for dijet production in this model is the same as for a DM mediator (see text).

Fig. 13 with a coupling $g'_q = g_q = 0.25$. Therefore, for these values of m_{DM} the limits on the mediator mass in Fig. 14 are identical to the limits on the Z' mass at $g'_q = 0.25$ in Fig. 13. Similarly, if $m_{\text{DM}} = 0$, the limits on the mediator mass in Fig. 14 are identical to the limits on the Z' mass at $g'_q = g_q / \sqrt{1 + 16 / (3N_f)} \approx 0.182$ in Fig. 13. Here N_f is the effective number of quark flavors contributing to the width of the resonance, $N_f = 5 + \sqrt{1 - 4m_t^2 / M_{\text{Med}}^2}$, where m_t is the top quark mass.

5.2 Limits on the coupling to quarks of a narrow DM mediator

In Fig. 15 limits are presented on the coupling g_q as a function of m_{DM} and M_{Med} . The limits on g_q decrease with increasing m_{DM} , again because the branching fraction to $q\bar{q}$ increases with m_{DM} . The minimum value of excluded g_q at a fixed value of M_{Med} is obtained for m_{DM} greater than $M_{\text{Med}}/2$.

In Figs. 13 and 15 we show exclusions from the narrow resonance search as a function of resonance mass and quark coupling up to a maximum coupling value of approximately 0.4, corresponding to a maximum resonance mass of 3.7 TeV. At larger values of coupling the natural width of the resonance influences significantly the observed width and our narrow resonance limits become noticeably less accurate. In the next section we quantify more precisely the accuracy of our narrow-resonance limits, extend them to larger widths, and extend the limits on a dark matter mediator to higher masses and couplings.

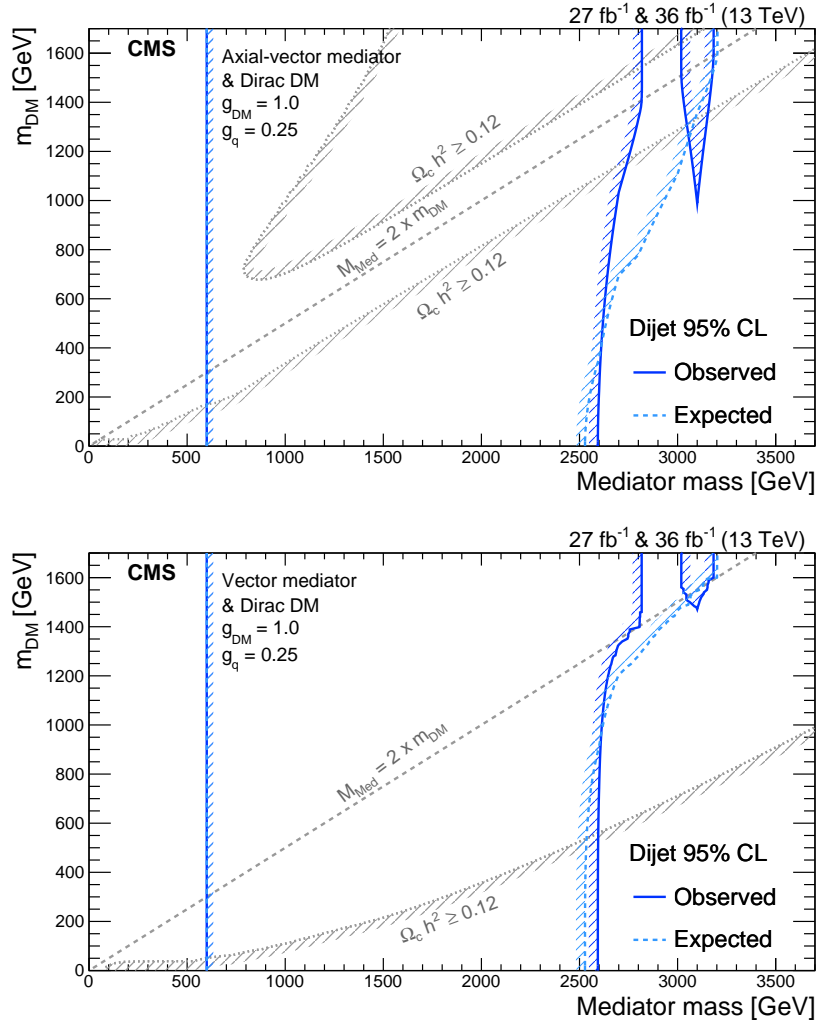


Figure 14: The 95% CL observed (solid) and expected (dashed) excluded regions in the plane of dark matter mass vs. mediator mass, for an axial-vector mediator (upper) and a vector mediator (lower), compared to the excluded regions where the abundance of DM exceeds the cosmological relic density (light gray). Following the recommendation of the LHC DM working group [31, 32], the exclusions are computed for Dirac DM and for a universal quark coupling $g_q = 0.25$ and for a DM coupling of $g_{\text{DM}} = 1.0$. It should also be noted that the excluded region strongly depends on the chosen coupling and model scenario. Therefore, the excluded regions and relic density contours shown in this plot are not applicable to other choices of coupling values or models.

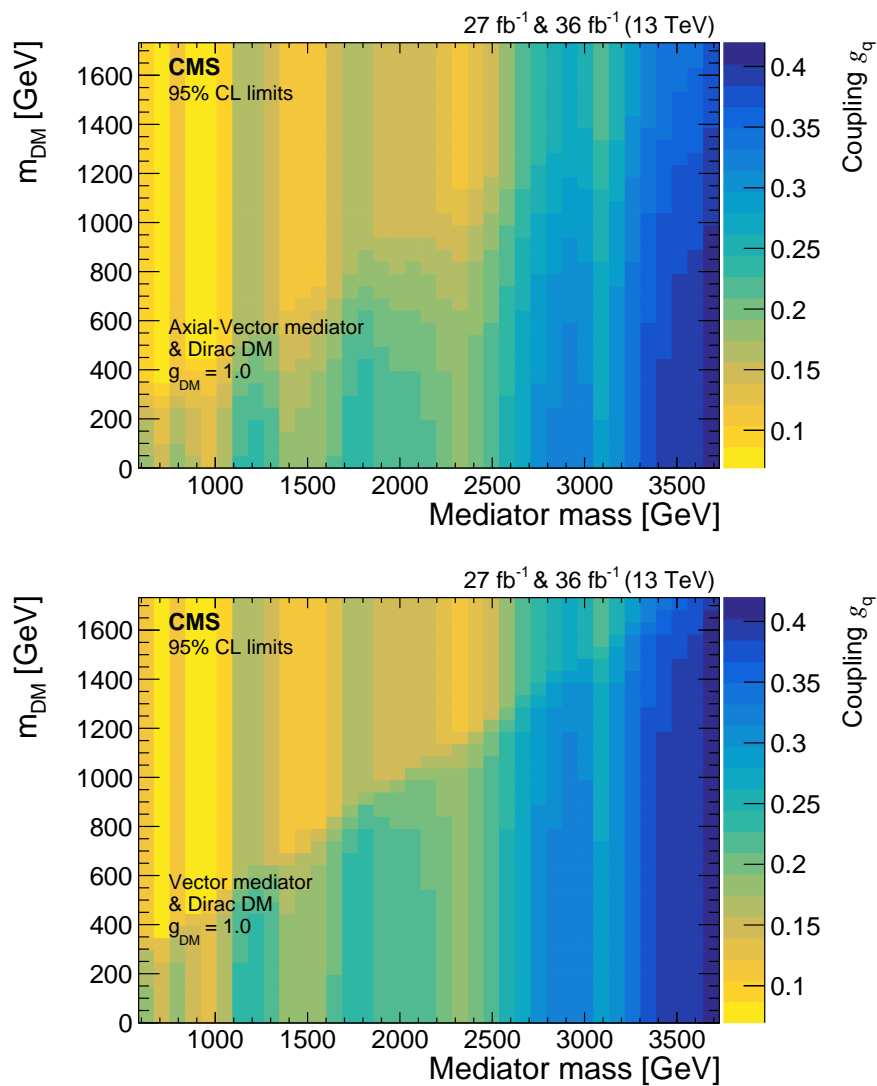


Figure 15: The 95% CL observed upper limits on a universal quark coupling g_q (color scale at right) in the plane of the dark matter particle mass versus mediator mass for an axial-vector mediator (upper) and a vector mediator (lower).

6 Limits on broad resonances

The search for narrow resonances described in the previous sections assumes the intrinsic resonance width Γ is negligible compared to the experimental dijet mass resolution. Here we extend the search to cover broader resonances, with the width up to 30% of the resonance mass M . This allows us to be sensitive to more models and larger couplings, and also quantifies the level of approximation within the narrow-resonance search by giving limits as an explicit function of Γ/M . We use the same dijet mass data and background parameterization as in the high-mass narrow resonance search. The shapes of broad resonances are then used to derive limits on such states decaying to qq and gg.

6.1 Breit–Wigner distributions

The shape of a broad resonance depends on the relationship between the width and the resonance mass, which in turn depends on the resonance spin and the decay channel. The subprocess cross section for a resonance with mass M as a function of di-parton mass m is described by a relativistic Breit–Wigner (e.g. Eq. (7.47) in Ref. [53]):

$$\hat{\sigma} \propto \frac{\pi}{m^2} \frac{[\Gamma^{(i)}M][\Gamma^{(f)}M]}{(m^2 - M^2)^2 + [\Gamma M]^2}, \quad (6)$$

where Γ is the total width and $\Gamma^{(i,f)}$ are the partial widths for the initial state i and final state f . To obtain the correct expression when the di-parton mass is far from the resonance mass, important for broad resonances, generators like PYTHIA 8 replace in Eq. (6) all ΓM terms with $\Gamma(m)m$ terms, where $\Gamma(m)$ is the width the resonance would have if its mass were m . This general prescription for modifying the Breit–Wigner distribution is defined at Eq. (47.58) in Ref. [68]. The replacement is done for the partial width terms in the numerator, as well as the full width term in the denominator, and the resulting di-parton mass dependence within the numerator significantly reduces the cross section at low values of m far from the resonance pole.

We consider explicitly the shapes of spin-1 resonances in the quark-quark channel and the shape of spin-2 resonances in the quark-quark and gluon-gluon channels. For a spin-1 Z' resonance in the quark-quark channel, both for the CP-even vector and the CP-odd axial-vector cases, the partial width is proportional to the resonance mass ($\Gamma \propto M$) [69] and generators make the well known replacement

$$\Gamma M \rightarrow \left(\frac{m^2}{M^2}\right) \Gamma M \quad (7)$$

for the terms $[\Gamma^{(i)}M]$, $[\Gamma^{(f)}M]$ and $[\Gamma M]$ in Eq. (6). The factor (m^2/M^2) in Eq. (7) converts the terms evaluated at the resonance mass to those evaluated at the di-parton mass for the case of widths proportional to mass, as discussed at Eq. (7.43) in Ref. [53]. For a spin-2 resonance, a CP-even tensor such as a graviton, the partial widths in both the gluon-gluon channel [69, 70] and the quark-quark channel [70] are proportional to the resonance mass cubed ($\Gamma \propto M^3$) and PYTHIA 8 makes the following replacement for an RS graviton:

$$\Gamma M \rightarrow \left(\frac{m^4}{M^4}\right) \Gamma M \quad (8)$$

for the above mentioned terms. The factor (m^4/M^4) in Eq. (8) converts the terms evaluated at the resonance mass to those evaluated at the di-parton mass for the case of widths proportional to mass cubed.

Applying the replacements in Eq. (7) and (8) to the $[\Gamma^{(i)}M][\Gamma^{(f)}M]$ in the numerator of the Breit–Wigner distribution results in an extra factor of $(m^2/M^2)(m^2/M^2) = m^4/M^4$ for a spin-2 resonance compared to a spin-1 resonance decaying to dijets. At low di-parton mass, $m \ll M$, the replacement in the denominator does not matter, and the replacement in the numerator will suppress the tail at low m for spin-2 resonances compared to spin-1 resonances, as can be seen in the figures in the next section. At high diparton mass, $m \gg M$, the replacement in the denominator will tend to cancel the replacement in the numerator and the high mass tail is not significantly affected by the replacement. This is true for the dijet decays of all spin-2 resonances calculated within effective field theory [69, 71]. We note that spin-2 resonances decaying to dijets are required to be CP-even, because the dijet decays of any spin-2 CP-odd resonances are suppressed [69].

Spin-0 resonances coupling directly to pairs of gluons (e.g. color-octet scalars) or to pairs of gluons through fermion loops (e.g. Higgs-like bosons) will have a partial width proportional to the resonance mass cubed [28, 69, 72] and should have a similar shape as a spin-2 resonance in the gluon-gluon channel. Spin-0 resonances coupling to quark-quark (e.g. Higgs-like bosons or scalar diquarks) will have a partial width proportional to the resonance mass [72, 73] and should have a similar shape as a spin-1 resonance in the quark-quark channel. Therefore, the three shapes we consider in Section 6.2, for spin-2 resonances coupling to quark-quark and gluon-gluon and for spin-1 resonances coupling to quark-quark, are sufficient to determine the shapes of all broad resonances decaying to quark-quark or gluon-gluon. We do not consider broad resonances with non-integer spin decaying to quark-gluon in this paper. Further discussion of the model dependence of the shape of broad resonances can be found in the Appendix of Ref. [8].

6.2 Resonance signal shapes and limits

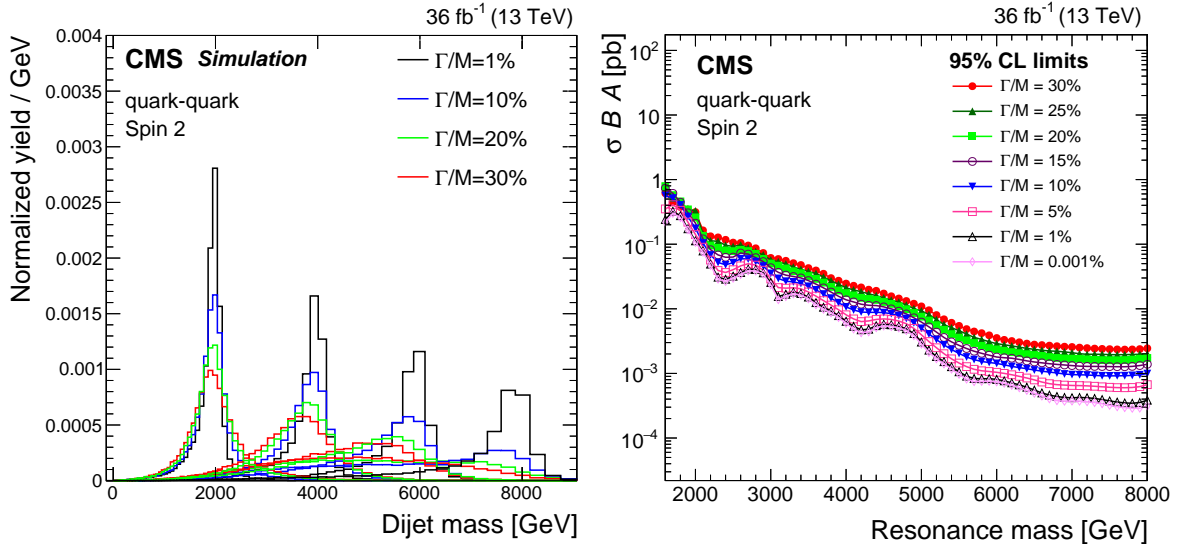


Figure 16: The resonance signal shapes (left) and observed 95% CL upper limits on the product of the cross section, branching fraction, and acceptance (right) for spin-2 resonances produced and decaying in the quark-quark channel are shown for various values of intrinsic width and resonance mass. The reconstructed dijet mass spectrum for these resonances is estimated from the PYTHIA 8 MC event generator, followed by the simulation of the CMS detector response.

In Figs. 16 and 17 we show resonance signal shapes and observed CMS limits for various

widths of spin-2 resonances modeled by an RS graviton signal in the quark-quark and gluon-gluon channels, respectively. The limits become less stringent as the resonance intrinsic width increases. While the extra factor of m^4/M^4 in the Breit-Wigner distribution discussed in the previous section suppresses the tail at low dijet mass for qq resonances, increased QCD radiation and a longer tail due to parton distributions partially compensates this effect for gg resonances. As a consequence and similar to narrow resonances, the broad resonances decaying to gg have a more pronounced tail at low mass, and hence the limits for these resonances are weaker than those for resonances decaying to qq. In Fig. 18 we show the signal shapes and limits for spin-1 resonances in the quark-quark channel. The spin-1 resonances in Fig. 18 do not contain the extra factor of m^4/M^4 in the Breit-Wigner distribution and are therefore significantly broader than the spin-2 qq resonances in Fig. 16. For the same reason, the limits in Fig. 18 are weaker than those in Fig. 16. In Fig. 18 we use a model of a vector DM mediator, and find the signal shapes and limits indistinguishable from an axial-vector model.

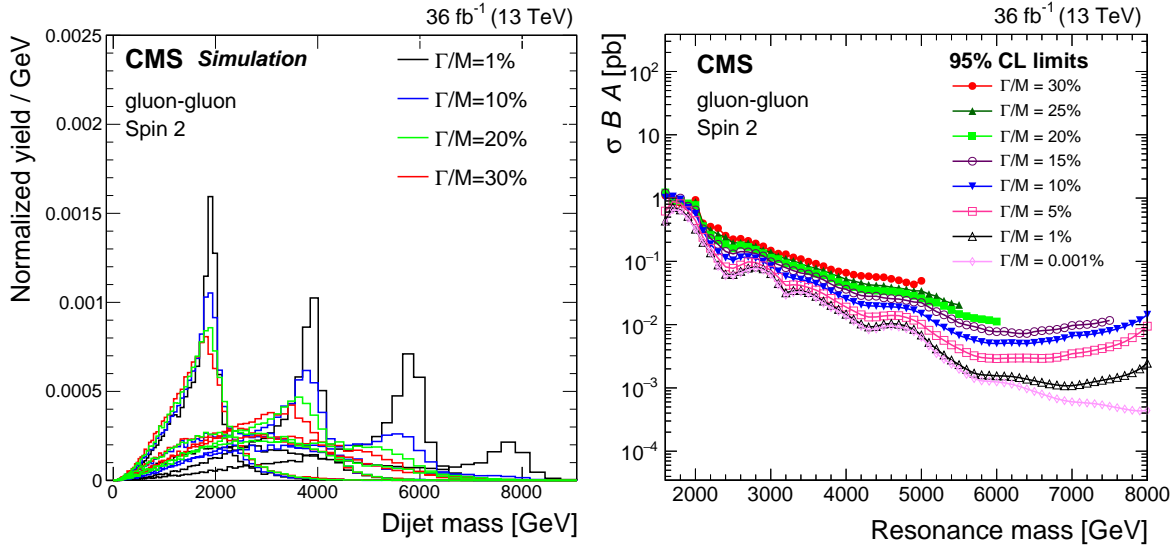


Figure 17: The resonance signal shapes (left) and observed 95% CL upper limits on the product of the cross section, branching fraction, and acceptance (right) for spin-2 resonances produced and decaying in the gluon-gluon channel are shown for various values of intrinsic width and resonance mass. The reconstructed dijet mass spectrum for these resonances is estimated from the PYTHIA 8 MC event generator, followed by the simulation of the CMS detector response.

6.3 Validity tests of the limits

The limits are calculated up to a resonance mass of 8 TeV but are only quoted up to the maximum resonance mass for which the presence of the low-mass tails in the signal shape does not significantly affect the limit value. For these quoted values, the limits on the resonance cross section are well understood, increasing monotonically as a function of resonance width at each value of resonance mass. To obtain this behavior in the limit, we find it is sufficient to require that the expected limit derived for a truncated shape agrees with that derived for the full shape within 15%. The truncated shape is cut off at a dijet mass equal to 70% of the nominal resonance mass, while the full shape is cut off at a dijet mass of 1.25 TeV. For both the truncated and the full limits, the cross section limit of the resonance signal is corrected for the acceptance of this requirement on the dijet mass in order to obtain limits on the total signal cross section. The difference between the expected limits using the full shape and the truncated shape is negligible for most resonance masses and widths, because the signal tail at low mass is

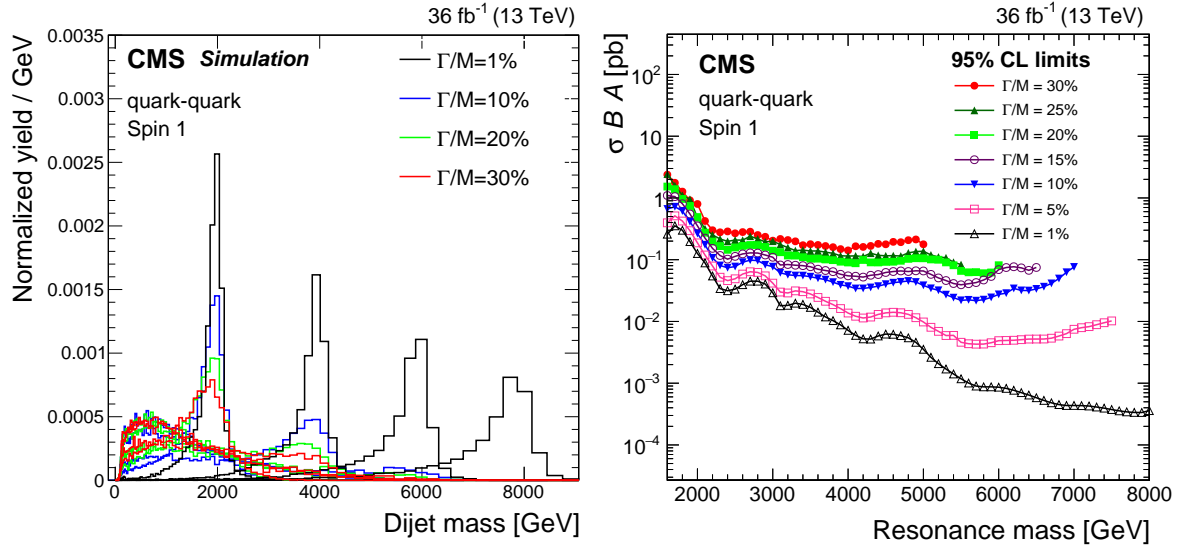


Figure 18: The resonance signal shapes (left) and observed 95% CL upper limits on the product of the cross section, branching fraction, and acceptance (right) for spin-1 resonances produced and decaying in the quark-quark channel are shown for various values of intrinsic width and resonance mass. The reconstructed dijet mass spectrum for these resonances is estimated from the PYTHIA 8 MC event generator, followed by the simulation of the CMS detector response.

insignificant compared to the steeply falling background. For some resonance masses beyond our maximum, the low dijet mass tail causes the limit to behave in an unphysical manner as a function of increasing width. This condition does not affect the maximum resonance mass presented for a spin-2 qq resonance in Fig.16, but it does restrict the maximum masses presented for a spin-2 gg resonance in Fig.17 and a vector resonance in Fig.18. For example, for a vector resonance, we find that the highest resonance mass that satisfies this condition is 5 TeV for a resonance with 30% width, 6 TeV for 20% width, 7 TeV for 10% width, and 8 TeV for a narrow resonance. It is useful to define the signal pseudo-significance distribution S/\sqrt{B} where S is the resonance signal and B is the QCD background. The signal pseudo-significance indicates sensitivity to the signal in the presence of background as a function of dijet mass, and has been used as an alternative method of evaluating the sensitivity of the search to the low mass tail. The maximum resonance mass values we present correspond to a 70% acceptance for the signal pseudo-significance, when the signal shape is truncated at 70% of the nominal resonance mass. This demonstrates that, for resonance masses and widths which satisfy our resonance mass condition, the signals are being constrained mainly by data in the dijet mass region near the resonance pole. Signal injection tests analogous to those already described for the narrow resonance search were repeated for the broad resonance search, and the bias in the extracted signal was again found to be negligible. As discussed in the previous CMS search for broad dijet resonances [8], our signal shapes consider only the s -channel process, which dominates the signal, and our results do not include the possible effects of the t -channel exchange of a new particle or the interference between the background and signal processes.

6.4 Limits on the coupling to quarks of a broad DM mediator

The cross section limits in Fig. 18 have been used to derive constraints on a DM mediator. The cross section for mediator production for $m_{\text{DM}} = 1$ GeV and $g_{\text{DM}} = 1$ is calculated at leading order using MADGRAPH5_aMC@NLO version 2.3.2 [74] for mediator masses within the range

$1.6 < M_{\text{Med}} < 4.1$ TeV in 0.1 TeV steps and for quark couplings within the range $0.1 < g_q < 1.0$ in 0.1 steps. For these choices the relationship between the width and g_q given in Ref. [31, 32] simplifies to

$$\Gamma_{\text{Med}} \approx \frac{(18g_q^2 + 1)M_{\text{Med}}}{12\pi}, \quad (9)$$

for both vector and axial-vector mediators.

For each mediator mass value, the predictions for the cross section for mediator production as a function of g_q are converted to a function of the width, using Eq. (9), and are then compared to our cross section limits from Fig. 18 to find the excluded values of g_q as a function of mass for a spin-1 resonance shown in Fig. 19. Also shown in Fig. 19 is the limit on g_q from the quark-

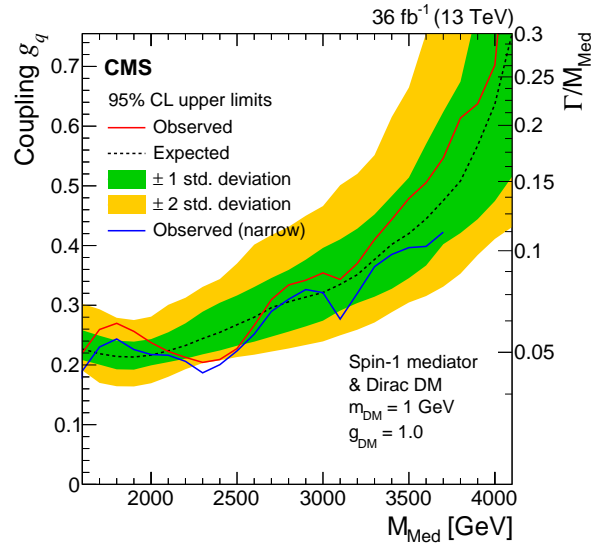


Figure 19: The 95% CL upper limits on the universal quark coupling g_q as a function of resonance mass for a vector mediator of interactions between quarks and DM particles. The right vertical axis shows the natural width of the mediator divided by its mass. The observed limits taking into account the natural width of the resonance are in red (upper solid curve), expected limits (dashed) and their variation at the 1 and 2 standard deviation levels (shaded bands) are shown. The observed limits from the narrow resonance search are in blue (lower solid curve), but are only valid for the width values up to approximately 10% of the resonance mass. The exclusions are computed for a spin-1 mediator and, Dirac DM particle with a mass $m_{\text{DM}} = 1$ GeV and a coupling $g_{\text{DM}} = 1.0$.

quark narrow resonance shape we used in the previous sections to set narrow-resonance limits. These are equal to the limits on g_q in Fig. 15 and are derived from the limits on g'_q in Fig. 13 using the formula

$$g_q = g'_q \sqrt{\frac{1}{2} + \sqrt{\frac{1}{4} + \frac{1}{18(g'_q)^2}}}. \quad (10)$$

Equation (10) is applicable for a narrow mediator with $g_{\text{DM}} = 1$ and mass much larger than the quark and DM particle masses. The quark-quark narrow-resonance limits are derived from a narrow spin-2 resonance shape, which is approximately the same as a spin-1 resonance shape for small values of g_q , and therefore in Fig. 19 at small values of g_q the narrow-resonance limits are roughly the same as the limits which take into account the width of the resonance. For resonance masses smaller than about 2.5 TeV, the acceptance of the dijet mass requirement

$m_{jj} > 1.25$ TeV is reduced by taking into account the resonance natural width, resulting in a small increase in the limits compared to the narrow-resonance limits, which can be seen in Fig. 19. At 3.7 TeV, the largest value of the resonance mass considered approximately valid for the narrow-resonance limits on g_q , the narrow-resonance limit is $g_q > 0.42$, while the more accurate limit taking into account the width for the spin-1 resonance is $g_q > 0.53$. The limits taking into account the natural width can be calculated up to a resonance mass of 4.1 TeV for a width up to 30% of the resonance mass. The limits from the narrow resonance search are approximately valid up to coupling values of about 0.4, corresponding to a width of 10%, while the limits taking into account the natural width of the resonance probe up to a coupling value of 0.76, corresponding to a natural width of 30%. We conclude that these limits on a vector DM mediator, taking into account the natural width of the resonance, improve on the accuracy of the narrow-width limits and extend them to larger values of the resonance mass and coupling to quarks.

7 Summary

Searches have been presented for resonances decaying into pairs of jets using proton-proton collision data collected at $\sqrt{s} = 13$ TeV corresponding to an integrated luminosity of up to 36 fb^{-1} . A low-mass search, for resonances with masses between 0.6 and 1.6 TeV, is performed based on events with dijets reconstructed at the trigger level from calorimeter information. A high-mass search, for resonances with masses above 1.6 TeV, is performed using dijets reconstructed offline with a particle-flow algorithm. The dijet mass spectra are observed to be smoothly falling distributions. In the analyzed data samples, there is no evidence for resonant particle production. Generic upper limits are presented on the product of the cross section, the branching fraction to dijets, and the acceptance for narrow quark-quark, quark-gluon, and gluon-gluon resonances that are applicable to any model of narrow dijet resonance production. String resonances with masses below 7.7 TeV are excluded at 95% confidence level, as are scalar diquarks below 7.2 TeV, axigluons and colorons below 6.1 TeV, excited quarks below 6.0 TeV, color-octet scalars below 3.4 TeV, W' bosons with the SM-like couplings below 3.3 TeV, Z' bosons with the SM-like couplings below 2.7 TeV, Randall–Sundrum gravitons below 1.8 TeV and in the range 1.9 to 2.5 TeV, and dark matter mediators below 2.6 TeV. The limits on both vector and axial-vector mediators, in a simplified model of interactions between quarks and dark matter particles, are presented as functions of dark matter particle mass. Searches are also presented for broad resonances, including for the first time spin-1 resonances with intrinsic widths as large as 30% of the resonance mass. The broad resonance search improves and extends the exclusions of a dark matter mediator to larger values of its mass and coupling to quarks. The narrow and broad resonance searches extend limits previously reported by CMS in the dijet channel, resulting in the most stringent constraints on many of the models considered.

Acknowledgments

We congratulate our colleagues in the CERN accelerator departments for the excellent performance of the LHC and thank the technical and administrative staffs at CERN and at other CMS institutes for their contributions to the success of the CMS effort. In addition, we gratefully acknowledge the computing centers and personnel of the Worldwide LHC Computing Grid for delivering so effectively the computing infrastructure essential to our analyses. Finally, we acknowledge the enduring support for the construction and operation of the LHC and the CMS detector provided by the following funding agencies: the Austrian Federal Ministry of Science, Research and Economy and the Austrian Science Fund; the Belgian Fonds de

la Recherche Scientifique, and Fonds voor Wetenschappelijk Onderzoek; the Brazilian Funding Agencies (CNPq, CAPES, FAPERJ, and FAPESP); the Bulgarian Ministry of Education and Science; CERN; the Chinese Academy of Sciences, Ministry of Science and Technology, and National Natural Science Foundation of China; the Colombian Funding Agency (COLCIENCIAS); the Croatian Ministry of Science, Education and Sport, and the Croatian Science Foundation; the Research Promotion Foundation, Cyprus; the Secretariat for Higher Education, Science, Technology and Innovation, Ecuador; the Ministry of Education and Research, Estonian Research Council via IUT23-4 and IUT23-6 and European Regional Development Fund, Estonia; the Academy of Finland, Finnish Ministry of Education and Culture, and Helsinki Institute of Physics; the Institut National de Physique Nucléaire et de Physique des Particules / CNRS, and Commissariat à l'Énergie Atomique et aux Énergies Alternatives / CEA, France; the Bundesministerium für Bildung und Forschung, Deutsche Forschungsgemeinschaft, and Helmholtz-Gemeinschaft Deutscher Forschungszentren, Germany; the General Secretariat for Research and Technology, Greece; the National Research, Development and Innovation Fund, Hungary; the Department of Atomic Energy and the Department of Science and Technology, India; the Institute for Studies in Theoretical Physics and Mathematics, Iran; the Science Foundation, Ireland; the Istituto Nazionale di Fisica Nucleare, Italy; the Ministry of Science, ICT and Future Planning, and National Research Foundation (NRF), Republic of Korea; the Lithuanian Academy of Sciences; the Ministry of Education, and University of Malaya (Malaysia); the Mexican Funding Agencies (BUAP, CINVESTAV, CONACYT, LNS, SEP, and UASLP-FAI); the Ministry of Business, Innovation and Employment, New Zealand; the Pakistan Atomic Energy Commission; the Ministry of Science and Higher Education and the National Science center, Poland; the Fundação para a Ciência e a Tecnologia, Portugal; JINR, Dubna; the Ministry of Education and Science of the Russian Federation, the Federal Agency of Atomic Energy of the Russian Federation, Russian Academy of Sciences and the Russian Foundation for Basic Research; the Ministry of Education, Science and Technological Development of Serbia; the Secretaría de Estado de Investigación, Desarrollo e Innovación, Programa Consolider-Ingenio 2010, Plan Estatal de Investigación Científica y Técnica y de Innovación 2013-2016, Plan de Ciencia, Tecnología e Innovación 2013-2017 del Principado de Asturias and Fondo Europeo de Desarrollo Regional, Spain; the Swiss Funding Agencies (ETH Board, ETH Zurich, PSI, SNF, UniZH, Canton Zurich, and SER); the Ministry of Science and Technology, Taipei; the Thailand Center of Excellence in Physics, the Institute for the Promotion of Teaching Science and Technology of Thailand, Special Task Force for Activating Research and the National Science and Technology Development Agency of Thailand; the Scientific and Technical Research Council of Turkey, and Turkish Atomic Energy Authority; the National Academy of Sciences of Ukraine, and State Fund for Fundamental Researches, Ukraine; the Science and Technology Facilities Council, UK; the US Department of Energy, and the US National Science Foundation.

Individuals have received support from the Marie-Curie program and the European Research Council and Horizon 2020 Grant, contract No. 675440 (European Union); the Leventis Foundation; the A. P. Sloan Foundation; the Alexander von Humboldt Foundation; the Belgian Federal Science Policy Office; the Fonds pour la Formation à la Recherche dans l'Industrie et dans l'Agriculture (FRRIA-Belgium); the Agentschap voor Innovatie door Wetenschap en Technologie (IWT-Belgium); the F.R.S.-FNRS and FWO (Belgium) under the "Excellence of Science - EOS" - be.h project n. 30820817; the Ministry of Education, Youth and Sports (MEYS) of the Czech Republic; the Lendület ("Momentum") program and the János Bolyai Research Scholarship of the Hungarian Academy of Sciences, the New National Excellence Program ÚNKP, the NKFI research grants 123842, 123959, 124845, 124850 and 125105 (Hungary); the Council of Scientific and Industrial Research, India; the HOMING PLUS program of the Foundation for Polish Science, cofinanced from European Union, Regional Development Fund, the Mo-

bility Plus program of the Ministry of Science and Higher Education, the National Science Center (Poland), contracts Harmonia 2014/14/M/ST2/00428, Opus 2014/13/B/ST2/02543, 2014/15/B/ST2/03998, and 2015/19/B/ST2/02861, Sonata-bis 2012/07/E/ST2/01406; the National Priorities Research Program by Qatar National Research Fund; the Programa de Excelencia María de Maeztu and the Programa Severo Ochoa del Principado de Asturias; the Thalys and Aristeia programs cofinanced by EU-ESF and the Greek NSRF; the Rachadapisek Sompot Fund for Postdoctoral Fellowship, Chulalongkorn University and the Chulalongkorn Academic into Its 2nd Century Project Advancement Project (Thailand); the Welch Foundation, contract C-1845; and the Weston Havens Foundation (USA).

References

- [1] M. Chala et al., “Constraining dark sectors with monojets and dijets”, *JHEP* **07** (2015) 089, doi:10.1007/JHEP07(2015)089, arXiv:1503.05916.
- [2] ATLAS Collaboration, “Search for low-mass dijet resonances using trigger-level jets with the ATLAS detector in pp collisions at $\sqrt{s} = 13$ TeV”, (2018). arXiv:1804.03496. Submitted to *Phys. Rev. Lett.*
- [3] ATLAS Collaboration, “Search for new phenomena in dijet events using 37 fb^{-1} of pp collision data collected at $\sqrt{s} = 13$ TeV with the ATLAS detector”, *Phys. Rev. D* **96** (2017) 052004, doi:10.1103/PhysRevD.96.052004, arXiv:1703.09127.
- [4] CMS Collaboration, “Search for dijet resonances in proton-proton collisions at $\sqrt{s} = 13$ TeV and constraints on dark matter and other models”, *Phys. Lett. B* **769** (2017) 520, doi:10.1016/j.physletb.2017.02.012, arXiv:1611.03568.
- [5] CMS Collaboration, “Search for narrow resonances decaying to dijets in proton-proton collisions at $\sqrt{s} = 13$ TeV”, *Phys. Rev. Lett.* **116** (2016) 071801, doi:10.1103/PhysRevLett.116.071801, arXiv:1512.01224.
- [6] ATLAS Collaboration, “Search for new phenomena in dijet mass and angular distributions from pp collisions at $\sqrt{s} = 13$ TeV with the ATLAS detector”, *Phys. Lett. B* **754** (2016) 302, doi:10.1016/j.physletb.2016.01.032, arXiv:1512.01530.
- [7] CMS Collaboration, “Search for narrow resonances in dijet final states at $\sqrt{s} = 8$ TeV with the novel CMS technique of data scouting”, *Phys. Rev. Lett.* **117** (2016) 031802, doi:10.1103/PhysRevLett.117.031802, arXiv:1604.08907.
- [8] CMS Collaboration, “Search for resonances and quantum black holes using dijet mass spectra in proton-proton collisions at $\sqrt{s} = 8$ TeV”, *Phys. Rev. D* **91** (2015) 052009, doi:10.1103/PhysRevD.91.052009, arXiv:1501.04198.
- [9] ATLAS Collaboration, “Search for new phenomena in the dijet mass distribution using pp collision data at $\sqrt{s} = 8$ TeV with the ATLAS detector”, *Phys. Rev. D* **91** (2015) 052007, doi:10.1103/PhysRevD.91.052007, arXiv:1407.1376.
- [10] CMS Collaboration, “Search for narrow resonances using the dijet mass spectrum in pp collisions at $\sqrt{s} = 8$ TeV”, *Phys. Rev. D* **87** (2013) 114015, doi:10.1103/PhysRevD.87.114015, arXiv:1302.4794.

- [11] CMS Collaboration, “Search for narrow resonances and quantum black holes in inclusive and b-tagged dijet mass spectra from pp collisions at $\sqrt{s} = 7$ TeV”, *JHEP* **01** (2013) 013, doi:10.1007/JHEP01(2013)013, arXiv:1210.2387.
- [12] ATLAS Collaboration, “Search for new physics in the dijet mass distribution using 1 fb^{-1} of pp collision data at $\sqrt{s} = 7$ TeV collected by the ATLAS detector”, *Phys. Lett. B* **708** (2012) 37, doi:10.1016/j.physletb.2012.01.035, arXiv:1108.6311.
- [13] ATLAS Collaboration, “ATLAS search for new phenomena in dijet mass and angular distributions using pp collisions at $\sqrt{s} = 7$ TeV”, *JHEP* **01** (2013) 029, doi:10.1007/JHEP01(2013)029, arXiv:1210.1718.
- [14] CMS Collaboration, “Search for resonances in the dijet mass spectrum from 7 TeV pp collisions at CMS”, *Phys. Lett. B* **704** (2011) 123, doi:10.1016/j.physletb.2011.09.015, arXiv:1107.4771.
- [15] ATLAS Collaboration, “Search for new physics in dijet mass and angular distributions in pp collisions at $\sqrt{s} = 7$ TeV measured with the ATLAS detector”, *New J. Phys.* **13** (2011) 053044, doi:10.1088/1367-2630/13/5/053044, arXiv:1103.3864.
- [16] CMS Collaboration, “Search for Dijet Resonances in 7 TeV pp Collisions at CMS”, *Phys. Rev. Lett.* **105** (2010) 211801, doi:10.1103/PhysRevLett.105.211801, arXiv:1010.0203. [Erratum doi:10.1103/PhysRevLett.106.029902].
- [17] ATLAS Collaboration, “Search for new particles in two-jet final states in 7 TeV proton-proton collisions with the ATLAS detector at the LHC”, *Phys. Rev. Lett.* **105** (2010) 161801, doi:10.1103/PhysRevLett.105.161801, arXiv:1008.2461.
- [18] R. M. Harris and K. Kousouris, “Searches for dijet resonances at hadron colliders”, *Int. J. Mod. Phys. A* **26** (2011) 5005, doi:10.1142/S0217751X11054905, arXiv:1110.5302.
- [19] S. Mukherjee, “Data Scouting : A New Trigger Paradigm”, in *5th Large Hadron Collider Physics Conference (LHCP 2017) Shanghai, China, May 15-20, 2017*. arXiv:1708.06925.
- [20] L. A. Anchordoqui et al., “Dijet signals for low mass strings at the Large Hadron Collider”, *Phys. Rev. Lett.* **101** (2008) 241803, doi:10.1103/PhysRevLett.101.241803, arXiv:0808.0497.
- [21] S. Cullen, M. Perelstein, and M. E. Peskin, “TeV strings and collider probes of large extra dimensions”, *Phys. Rev. D* **62** (2000) 055012, doi:10.1103/PhysRevD.62.055012, arXiv:hep-ph/0001166.
- [22] J. L. Hewett and T. G. Rizzo, “Low-energy phenomenology of superstring-inspired E_6 models”, *Phys. Rept.* **183** (1989) 193, doi:10.1016/0370-1573(89)90071-9.
- [23] U. Baur, I. Hinchliffe, and D. Zeppenfeld, “Excited quark production at hadron colliders”, *Int. J. Mod. Phys. A* **02** (1987) 1285, doi:10.1142/S0217751X87000661.
- [24] U. Baur, M. Spira, and P. M. Zerwas, “Excited-quark and -lepton production at hadron colliders”, *Phys. Rev. D* **42** (1990) 815, doi:10.1103/PhysRevD.42.815.
- [25] P. H. Frampton and S. L. Glashow, “Chiral color: An alternative to the standard model”, *Phys. Lett. B* **190** (1987) 157, doi:10.1016/0370-2693(87)90859-8.

-
- [26] E. H. Simmons, “Coloron phenomenology”, *Phys. Rev. D* **55** (1997) 1678, doi:10.1103/PhysRevD.55.1678, arXiv:hep-ph/9608269.
- [27] T. Han, I. Lewis, and Z. Liu, “Colored resonant signals at the LHC: largest rate and simplest topology”, *JHEP* **12** (2010) 085, doi:10.1007/JHEP12(2010)085, arXiv:1010.4309.
- [28] R. S. Chivukula, E. H. Simmons, and N. Vignaroli, “Distinguishing dijet resonances at the LHC”, *Phys. Rev. D* **91** (2015) 055019, doi:10.1103/PhysRevD.91.055019, arXiv:1412.3094.
- [29] E. Eichten, I. Hinchliffe, K. D. Lane, and C. Quigg, “Supercollider physics”, *Rev. Mod. Phys.* **56** (1984) 579, doi:10.1103/RevModPhys.56.579.
- [30] L. Randall and R. Sundrum, “An alternative to compactification”, *Phys. Rev. Lett.* **83** (1999) 4690, doi:10.1103/PhysRevLett.83.4690, arXiv:hep-th/9906064.
- [31] A. Boveia et al., “Recommendations on presenting LHC searches for missing transverse energy signals using simplified s -channel models of dark matter”, (2016). arXiv:1603.04156.
- [32] J. Abdallah et al., “Simplified models for dark matter searches at the LHC”, *Phys. Dark Univ.* **9-10** (2015) 8, doi:10.1016/j.dark.2015.08.001, arXiv:1506.03116.
- [33] B. A. Dobrescu and F. Yu, “Coupling-mass mapping of dijet peak searches”, *Phys. Rev. D* **88** (2013) 035021, doi:10.1103/PhysRevD.88.035021, arXiv:1306.2629. [Erratum: doi:10.1103/PhysRevD.90.079901].
- [34] CMS Collaboration, “The CMS experiment at the CERN LHC”, *JINST* **3** (2008) S08004, doi:10.1088/1748-0221/3/08/S08004.
- [35] CMS Collaboration, “Particle-flow reconstruction and global event description with the CMS detector”, *JINST* **12** (2017) P10003, doi:10.1088/1748-0221/12/10/P10003, arXiv:1706.04965.
- [36] M. Cacciari and G. P. Salam, “Dispelling the N^3 myth for the k_T jet-finder”, *Phys. Lett. B* **641** (2006) 57, doi:10.1016/j.physletb.2006.08.037, arXiv:hep-ph/0512210.
- [37] M. Cacciari, G. P. Salam, and G. Soyez, “The anti- k_T jet clustering algorithm”, *JHEP* **04** (2008) 063, doi:10.1088/1126-6708/2008/04/063, arXiv:0802.1189.
- [38] M. Cacciari, G. P. Salam, and G. Soyez, “FastJet user manual”, *Eur. Phys. J. C* **72** (2012) 1896, doi:10.1140/epjc/s10052-012-1896-2, arXiv:1111.6097.
- [39] M. Cacciari and G. P. Salam, “Pileup subtraction using jet areas”, *Phys. Lett. B* **659** (2008) 119, doi:10.1016/j.physletb.2007.09.077, arXiv:0707.1378.
- [40] CMS Collaboration, “Jet energy scale and resolution in the CMS experiment in pp collisions at 8 TeV”, *JINST* **12** (2017) P02014, doi:10.1088/1748-0221/12/02/P02014, arXiv:1607.03663.
- [41] CMS Collaboration, “The CMS trigger system”, *JINST* **12** (2017) P01020, doi:10.1088/1748-0221/12/01/P01020, arXiv:1609.02366.
- [42] CMS Collaboration, “Jet algorithms performance in 13 TeV data”, CMS Physics Analysis Summary CMS-PAS-JME-16-003, 2017.

- [43] D. Krohn, J. Thaler, and L.-T. Wang, “Jet trimming”, *JHEP* **02** (2010) 084, doi:10.1007/JHEP02(2010)084.
- [44] T. Sjöstrand, S. Mrenna, and P. Skands, “A brief introduction to PYTHIA 8.1”, *Comp. Phys. Comm.* **178** (2008) 852, doi:10.1016/j.cpc.2008.01.036, arXiv:0710.3820.
- [45] CMS Collaboration, “Event generator tunes obtained from underlying event and multiparton scattering measurements”, *Eur. Phys. J. C* **76** (2016) 155, doi:10.1140/epjc/s10052-016-3988-x, arXiv:1512.00815.
- [46] P. Skands, S. Carrazza, and J. Rojo, “Tuning PYTHIA 8.1: the Monash 2013 tune”, *Eur. Phys. J. C* **74** (2014) 3024, doi:10.1140/epjc/s10052-014-3024-y, arXiv:1404.5630.
- [47] GEANT4 Collaboration, “GEANT4 — a simulation toolkit”, *Nucl. Instr. Meth. A* **506** (2003) 250, doi:10.1016/S0168-9002(03)01368-8.
- [48] S. Alioli, P. Nason, C. Oleari, and E. Re, “A general framework for implementing NLO calculations in shower Monte Carlo programs: the POWHEG BOX”, *JHEP* **06** (2010) 043, doi:10.1007/JHEP06(2010)043, arXiv:1002.2581.
- [49] S. Alioli et al., “Jet pair production in POWHEG”, *JHEP* **04** (2011) 081, doi:10.1007/JHEP04(2011)081, arXiv:1012.3380.
- [50] NNPDF Collaboration, “Parton distributions for the LHC Run II”, *JHEP* **04** (2015) 040, doi:10.1007/JHEP04(2015)040, arXiv:1410.8849.
- [51] CDF Collaboration, “Search for new particles decaying into dijets in proton-antiproton collisions at $\sqrt{s} = 1.96$ TeV”, *Phys. Rev. D* **79** (2009) 112002, doi:10.1103/PhysRevD.79.112002, arXiv:0812.4036.
- [52] R. G. Lomax and D. L. Hahs-Vaughn, “Statistical concepts: A second course”. Routledge Academic, London, 2007.
- [53] T. Sjöstrand, S. Mrenna, and P. Z. Skands, “PYTHIA 6.4 physics and manual”, *JHEP* **05** (2006) 026, doi:10.1088/1126-6708/2006/05/026, arXiv:hep-ph/0603175.
- [54] S. P. Martin, “Signal-background interference for a singlet spin-0 digluon resonance at the LHC”, *Phys. Rev. D* **94** (2016) 035003, doi:10.1103/PhysRevD.94.035003, arXiv:1606.03026.
- [55] CMS Collaboration, “CMS luminosity measurements for the 2016 data taking period”, CMS Physics Analysis Summary CMS-PAS-LUM-17-001, 2017.
- [56] G. Cowan, K. Cranmer, E. Gross, and O. Vitells, “Asymptotic formulae for likelihood-based tests of new physics”, *Eur. Phys. J. C* **71** (2011) 1554, doi:10.1140/epjc/s10052-011-1554-0, arXiv:1007.1727. [Erratum: doi:10.1140/epjc/s10052-013-2501-z].
- [57] T. Junk, “Confidence level computation for combining searches with small statistics”, *Nucl. Instr. Meth. A* **434** (1999) 435, doi:10.1016/S0168-9002(99)00498-2, arXiv:hep-ex/9902006.

-
- [58] A. L. Read, "Presentation of search results: the CL_s technique", *J. Phys. G* **28** (2002) 2693, doi:10.1088/0954-3899/28/10/313.
- [59] LHC Higgs Combination Group, "Procedure for the LHC Higgs boson search combination in Summer 2011", Technical Report CMS-NOTE-2011-005, ATL-PHYS-PUB-2011-11, 2011.
- [60] J. Pumplin et al., "New generation of parton distributions with uncertainties from global QCD analysis", *JHEP* **07** (2002) 012, doi:10.1088/1126-6708/2002/07/012, arXiv:hep-ph/0201195.
- [61] V. D. Barger and R. J. N. Phillips, "Collider Physics, Updated Edition, Frontiers in Physics Volume 71". Westview Press, Boulder, Colorado, 1996. ISBN 0-201-14945-1,
- [62] R. S. Chivukula, E. H. Simmons, A. Farzinnia, and J. Ren, "Hadron collider production of massive color-octet vector bosons at next-to-leading order", *Phys. Rev. D* **87** (2013) 094011, doi:10.1103/PhysRevD.87.094011, arXiv:1303.1120.
- [63] D. N. Spergel et al., "Three-Year Wilkinson Microwave Anisotropy Probe (WMAP) Observations: Implications for Cosmology", *Astrophys. J. Suppl.* **170** (2007) 377, doi:10.1086/513700, arXiv:astro-ph/0603449.
- [64] Planck Collaboration, "Planck 2013 results. XVI. Cosmological parameters", *Astron. Astrophys.* **571** (2014) A16, doi:10.1051/0004-6361/201321591, arXiv:1303.5076.
- [65] M. Backović, K. Kong, and M. McCaskey, "MadDM v.1.0: Computation of Dark Matter Relic Abundance Using MadGraph5", *Phys. Dark Univ.* **5** (2014) 18, doi:10.1016/j.dark.2014.04.001, arXiv:1308.4955.
- [66] M. Backović et al., "Direct detection of dark matter with MadDM v.2.0", *Phys. Dark Univ.* **9** (2015) 37, doi:10.1016/j.dark.2015.09.001, arXiv:1505.04190.
- [67] T. du Pree, K. Hahn, P. Harris, and C. Roskas, "Cosmological constraints on dark matter models for collider searches", (2016). arXiv:1603.08525.
- [68] Particle Data Group Collaboration, "Review of particle physics", *Chin. Phys. C* **40** (2016) 100001, doi:10.1088/1674-1137/40/10/100001.
- [69] H. M. Lee, D. Kim, K. Kong, and S. C. Park, "Diboson excesses demystified in effective field theory approach", *JHEP* **11** (2015) 150, doi:10.1007/JHEP11(2015)150, arXiv:1507.06312.
- [70] J. Bijnens et al., "QCD signatures of narrow graviton resonances in hadron colliders", *Phys. Lett. B* **503** (2001) 341, doi:10.1016/S0370-2693(01)00238-6, arXiv:hep-ph/0101316.
- [71] T. Han, J. D. Lykken, and R.-J. Zhang, "Kaluza-Klein states from large extra dimensions", *Phys. Rev. D* **59** (1999) 105006, doi:10.1103/PhysRevD.59.105006, arXiv:hep-ph/9811350.
- [72] J. Ellis, M. K. Gaillard, and D. V. Nanopoulos, "A phenomenological profile of the Higgs boson", *Nucl. Phys. B* **106** (1976) 292, doi:10.1016/0550-3213(76)90382-5.

-
- [73] O. Çakir and M. Şahin, “Resonant production of diquarks at high energy pp , ep and e^+e^- colliders”, *Phys. Rev. D* **72** (2005) 115011, doi:10.1103/PhysRevD.72.115011, arXiv:hep-ph/0508205.
- [74] J. Alwall et al., “The automated computation of tree-level and next-to-leading order differential cross sections, and their matching to parton shower simulations”, *JHEP* **07** (2014) 079, doi:10.1007/JHEP07(2014)079, arXiv:1405.0301.

A The CMS Collaboration

Yerevan Physics Institute, Yerevan, Armenia

A.M. Sirunyan, A. Tumasyan

Institut für Hochenergiephysik, Wien, Austria

W. Adam, F. Ambrogio, E. Asilar, T. Bergauer, J. Brandstetter, E. Brondolin, M. Dragicevic, J. Erö, A. Escalante Del Valle, M. Flechl, M. Friedl, R. Frühwirth¹, V.M. Ghete, J. Grossmann, J. Hrubec, M. Jeitler¹, A. König, N. Krammer, I. Krätschmer, D. Liko, T. Madlener, I. Mikulec, E. Pree, N. Rad, H. Rohringer, J. Schieck¹, R. Schöfbeck, M. Spanring, D. Spitzbart, A. Taurok, W. Waltenberger, J. Wittmann, C.-E. Wulz¹, M. Zarucki

Institute for Nuclear Problems, Minsk, Belarus

V. Chekhovsky, V. Mossolov, J. Suarez Gonzalez

Universiteit Antwerpen, Antwerpen, Belgium

E.A. De Wolf, D. Di Croce, X. Janssen, J. Lauwers, M. Pieters, M. Van De Klundert, H. Van Haevermaet, P. Van Mechelen, N. Van Remortel

Vrije Universiteit Brussel, Brussel, Belgium

S. Abu Zeid, F. Blekman, J. D'Hondt, I. De Bruyn, J. De Clercq, K. Deroover, G. Flouris, D. Lontkovskyi, S. Lowette, I. Marchesini, S. Moortgat, L. Moreels, Q. Python, K. Skovpen, S. Tavernier, W. Van Doninck, P. Van Mulders, I. Van Parijs

Université Libre de Bruxelles, Bruxelles, Belgium

D. Beghin, B. Bilin, H. Brun, B. Clerboux, G. De Lentdecker, H. Delannoy, B. Dorney, G. Fasanella, L. Favart, R. Goldouzian, A. Grebenyuk, A.K. Kalsi, T. Lenzi, J. Luetic, T. Seva, E. Starling, C. Vander Velde, P. Vanlaer, D. Vannerom, R. Yonamine

Ghent University, Ghent, Belgium

T. Cornelis, D. Dobur, A. Fagot, M. Gul, I. Khvastunov², D. Poyraz, C. Roskas, D. Trocino, M. Tytgat, W. Verbeke, B. Vermassen, M. Vit, N. Zaganidis

Université Catholique de Louvain, Louvain-la-Neuve, Belgium

H. Bakhshiansohi, O. Bondu, S. Brochet, G. Bruno, C. Caputo, A. Caudron, P. David, S. De Visscher, C. Delaere, M. Delcourt, B. Francois, A. Giammanco, G. Krintiras, V. Lemaitre, A. Magitteri, A. Mertens, M. Musich, K. Piotrkowski, L. Quertenmont, A. Saggio, M. Vidal Marono, S. Wertz, J. Zobec

Centro Brasileiro de Pesquisas Fisicas, Rio de Janeiro, Brazil

W.L. Aldá Júnior, F.L. Alves, G.A. Alves, L. Brito, G. Correia Silva, C. Hensel, A. Moraes, M.E. Pol, P. Rebello Teles

Universidade do Estado do Rio de Janeiro, Rio de Janeiro, Brazil

E. Belchior Batista Das Chagas, W. Carvalho, J. Chinellato³, E. Coelho, E.M. Da Costa, G.G. Da Silveira⁴, D. De Jesus Damiao, S. Fonseca De Souza, H. Malbouisson, M. Medina Jaime⁵, M. Melo De Almeida, C. Mora Herrera, L. Mundim, H. Nogima, L.J. Sanchez Rosas, A. Santoro, A. Sznajder, M. Thiel, E.J. Tonelli Manganote³, F. Torres Da Silva De Araujo, A. Vilela Pereira

Universidade Estadual Paulista ^a, Universidade Federal do ABC ^b, São Paulo, Brazil

S. Ahuja^a, C.A. Bernardes^a, L. Calligaris^a, T.R. Fernandez Perez Tomei^a, E.M. Gregores^b, P.G. Mercadante^b, S.F. Novaes^a, SandraS. Padula^a, D. Romero Abad^b, J.C. Ruiz Vargas^a

Institute for Nuclear Research and Nuclear Energy, Bulgarian Academy of Sciences, Sofia, Bulgaria

A. Aleksandrov, R. Hadjiiska, P. Iaydjiev, A. Marinov, M. Misheva, M. Rodozov, M. Shopova, G. Sultanov

University of Sofia, Sofia, Bulgaria

A. Dimitrov, L. Litov, B. Pavlov, P. Petkov

Beihang University, Beijing, China

W. Fang⁶, X. Gao⁶, L. Yuan

Institute of High Energy Physics, Beijing, China

M. Ahmad, J.G. Bian, G.M. Chen, H.S. Chen, M. Chen, Y. Chen, C.H. Jiang, D. Leggat, H. Liao, Z. Liu, F. Romeo, S.M. Shaheen, A. Spiezia, J. Tao, C. Wang, Z. Wang, E. Yazgan, H. Zhang, J. Zhao

State Key Laboratory of Nuclear Physics and Technology, Peking University, Beijing, China

Y. Ban, G. Chen, J. Li, Q. Li, S. Liu, Y. Mao, S.J. Qian, D. Wang, Z. Xu

Tsinghua University, Beijing, China

Y. Wang

Universidad de Los Andes, Bogota, Colombia

C. Avila, A. Cabrera, C.A. Carrillo Montoya, L.F. Chaparro Sierra, C. Florez, C.F. González Hernández, M.A. Segura Delgado

University of Split, Faculty of Electrical Engineering, Mechanical Engineering and Naval Architecture, Split, Croatia

B. Courbon, N. Godinovic, D. Lelas, I. Puljak, P.M. Ribeiro Cipriano, T. Sculac

University of Split, Faculty of Science, Split, Croatia

Z. Antunovic, M. Kovac

Institute Rudjer Boskovic, Zagreb, Croatia

V. Brigljevic, D. Ferencek, K. Kadija, B. Mesic, A. Starodumov⁷, T. Susa

University of Cyprus, Nicosia, Cyprus

M.W. Ather, A. Attikis, G. Mavromanolakis, J. Mousa, C. Nicolaou, F. Ptochos, P.A. Razis, H. Rykaczewski

Charles University, Prague, Czech Republic

M. Finger⁸, M. Finger Jr.⁸

Universidad San Francisco de Quito, Quito, Ecuador

E. Carrera Jarrin

Academy of Scientific Research and Technology of the Arab Republic of Egypt, Egyptian Network of High Energy Physics, Cairo, Egypt

Y. Assran^{9,10}, S. Elgammal¹⁰, S. Khalil¹¹

National Institute of Chemical Physics and Biophysics, Tallinn, Estonia

S. Bhowmik, R.K. Dewanjee, M. Kadastik, L. Perrini, M. Raidal, C. Veelken

Department of Physics, University of Helsinki, Helsinki, Finland

P. Eerola, H. Kirschenmann, J. Pekkanen, M. Voutilainen

Helsinki Institute of Physics, Helsinki, Finland

J. Havukainen, J.K. Heikkilä, T. Järvinen, V. Karimäki, R. Kinnunen, T. Lampén, K. Lassila-Perini, S. Laurila, S. Lehti, T. Lindén, P. Luukka, T. Mäenpää, H. Siikonen, E. Tuominen, J. Tuominiemi

Lappeenranta University of Technology, Lappeenranta, Finland

T. Tuuva

IRFU, CEA, Université Paris-Saclay, Gif-sur-Yvette, France

M. Besancon, F. Couderc, M. Dejardin, D. Denegri, J.L. Faure, F. Ferri, S. Ganjour, S. Ghosh, A. Givernaud, P. Gras, G. Hamel de Monchenault, P. Jarry, C. Leloup, E. Locci, M. Machet, J. Malcles, G. Negro, J. Rander, A. Rosowsky, M.Ö. Sahin, M. Titov

Laboratoire Leprince-Ringuet, Ecole polytechnique, CNRS/IN2P3, Université Paris-Saclay, Palaiseau, France

A. Abdulsalam¹², C. Amendola, I. Antropov, S. Baffioni, F. Beaudette, P. Busson, L. Cadamuro, C. Charlot, R. Granier de Cassagnac, M. Jo, I. Kucher, S. Lisniak, A. Lobanov, J. Martin Blanco, M. Nguyen, C. Ochando, G. Ortona, P. Paganini, P. Pigard, R. Salerno, J.B. Sauvan, Y. Sirois, A.G. Stahl Leiton, Y. Yilmaz, A. Zabi, A. Zghiche

Université de Strasbourg, CNRS, IPHC UMR 7178, Strasbourg, France

J.-L. Agram¹³, J. Andrea, D. Bloch, J.-M. Brom, E.C. Chabert, C. Collard, E. Conte¹³, X. Coubez, F. Drouhin¹³, J.-C. Fontaine¹³, D. Gelé, U. Goerlach, M. Jansová, P. Juillot, A.-C. Le Bihan, N. Tonon, P. Van Hove

Centre de Calcul de l'Institut National de Physique Nucleaire et de Physique des Particules, CNRS/IN2P3, Villeurbanne, France

S. Gadrat

Université de Lyon, Université Claude Bernard Lyon 1, CNRS-IN2P3, Institut de Physique Nucléaire de Lyon, Villeurbanne, France

S. Beauceron, C. Bernet, G. Boudoul, N. Chanon, R. Chierici, D. Contardo, P. Depasse, H. El Mamouni, J. Fay, L. Finco, S. Gascon, M. Gouzevitch, G. Grenier, B. Ille, F. Lagarde, I.B. Laktineh, H. Lattaud, M. Lethuillier, L. Mirabito, A.L. Pequegnot, S. Perries, A. Popov¹⁴, V. Sordini, M. Vander Donckt, S. Viret, S. Zhang

Georgian Technical University, Tbilisi, Georgia

T. Toriashvili¹⁵

Tbilisi State University, Tbilisi, Georgia

Z. Tsamalaidze⁸

RWTH Aachen University, I. Physikalisches Institut, Aachen, Germany

C. Autermann, L. Feld, M.K. Kiesel, K. Klein, M. Lipinski, M. Preuten, M.P. Rauch, C. Schomakers, J. Schulz, M. Teroerde, B. Wittmer, V. Zhukov¹⁴

RWTH Aachen University, III. Physikalisches Institut A, Aachen, Germany

A. Albert, D. Duchardt, M. Endres, M. Erdmann, S. Erdweg, T. Esch, R. Fischer, A. Güth, T. Hebbeker, C. Heidemann, K. Hoepfner, S. Knutzen, M. Merschmeyer, A. Meyer, P. Millet, S. Mukherjee, T. Pook, M. Radziej, H. Reithler, M. Rieger, F. Scheuch, D. Teyssier, S. Thüer

RWTH Aachen University, III. Physikalisches Institut B, Aachen, Germany

G. Flügge, B. Kargoll, T. Kress, A. Künsken, T. Müller, A. Nehr Korn, A. Nowack, C. Pistone, O. Pooth, A. Stahl¹⁶

Deutsches Elektronen-Synchrotron, Hamburg, Germany

M. Aldaya Martin, T. Arndt, C. Asawatangtrakuldee, K. Beernaert, O. Behnke, U. Behrens, A. Bermúdez Martínez, A.A. Bin Anuar, K. Borras¹⁷, V. Botta, A. Campbell, P. Connor, C. Contreras-Campana, F. Costanza, V. Danilov, A. De Wit, C. Diez Pardos, D. Domínguez Damiani, G. Eckerlin, D. Eckstein, T. Eichhorn, A. Elwood, E. Eren, E. Gallo¹⁸, J. Garay Garcia, A. Geiser, J.M. Grados Luyando, A. Grohsjean, P. Gunnellini, M. Guthoff, A. Harb, J. Hauk, H. Jung, M. Kasemann, J. Keaveney, C. Kleinwort, J. Knolle, I. Korol, D. Krücker, W. Lange, A. Lelek, T. Lenz, K. Lipka, W. Lohmann¹⁹, R. Mankel, I.-A. Melzer-Pellmann, A.B. Meyer, M. Meyer, M. Missiroli, G. Mittag, J. Mnich, A. Mussgiller, D. Pitzl, A. Raspereza, M. Savitskyi, P. Saxena, R. Shevchenko, N. Stefaniuk, H. Tholen, G.P. Van Onsem, R. Walsh, Y. Wen, K. Wichmann, C. Wissing, O. Zenaiev

University of Hamburg, Hamburg, Germany

R. Aggleton, S. Bein, V. Blobel, M. Centis Vignali, T. Dreyer, E. Garutti, D. Gonzalez, J. Haller, A. Hinzmann, M. Hoffmann, A. Karavdina, G. Kasieczka, R. Klanner, R. Kogler, N. Kovalchuk, S. Kurz, V. Kutzner, J. Lange, D. Marconi, J. Multhaupt, M. Niedziela, D. Nowatschin, T. Peiffer, A. Perieanu, A. Reimers, C. Scharf, P. Schleper, A. Schmidt, S. Schumann, J. Schwandt, J. Sonneveld, H. Stadie, G. Steinbrück, F.M. Stober, M. Stöver, D. Troendle, E. Usai, A. Vanhoefer, B. Vormwald

Karlsruher Institut fuer Technology

M. Akbiyik, C. Barth, M. Baselga, S. Baur, E. Butz, R. Caspart, T. Chwalek, F. Colombo, W. De Boer, A. Dierlamm, N. Faltermann, B. Freund, R. Friese, M. Giffels, M.A. Harrendorf, F. Hartmann¹⁶, S.M. Heindl, U. Husemann, F. Kassel¹⁶, S. Kudella, H. Mildner, M.U. Mozer, Th. Müller, M. Plagge, G. Quast, K. Rabbertz, M. Schröder, I. Shvetsov, G. Sieber, H.J. Simonis, R. Ulrich, S. Wayand, M. Weber, T. Weiler, S. Williamson, C. Wöhrmann, R. Wolf

Institute of Nuclear and Particle Physics (INPP), NCSR Demokritos, Aghia Paraskevi, Greece

G. Anagnostou, G. Daskalakis, T. Gerasis, A. Kyriakis, D. Loukas, I. Topsis-Giotis

National and Kapodistrian University of Athens, Athens, Greece

M. Diamantopoulou, D. Karasavvas, G. Karathanasis, S. Kesisoglou, A. Panagiotou, N. Saoulidou, E. Tziaferi

National Technical University of Athens, Athens, Greece

K. Kousouris, I. Papakrivopoulos

University of Ioánnina, Ioánnina, Greece

I. Evangelou, C. Foudas, P. Giannelis, P. Katsoulis, P. Kokkas, S. Mallios, N. Manthos, I. Papadopoulos, E. Paradas, J. Strologas, F.A. Triantis, D. Tsitsonis

MTA-ELTE Lendület CMS Particle and Nuclear Physics Group, Eötvös Loránd University, Budapest, Hungary

M. Csanad, N. Filipovic, G. Pasztor, O. Surányi, G.I. Veres

Wigner Research Centre for Physics, Budapest, Hungary

G. Bencze, C. Hajdu, D. Horvath²⁰, Á. Hunyadi, F. Sikler, T.Á. Vámi, V. Veszpremi, G. Vesztergombi[†]

Institute of Nuclear Research ATOMKI, Debrecen, Hungary

N. Beni, S. Czellar, J. Karancsi²², A. Makovec, J. Molnar, Z. Szillasi

Institute of Physics, University of Debrecen, Debrecen, Hungary

M. Bartók²¹, P. Raics, Z.L. Trocsanyi, B. Ujvari

Indian Institute of Science (IISc), Bangalore, India

S. Choudhury, J.R. Komaragiri

National Institute of Science Education and Research, HBNI, Bhubaneswar, India

S. Bahinipati²³, P. Mal, K. Mandal, A. Nayak²⁴, D.K. Sahoo²³, S.K. Swain

Panjab University, Chandigarh, India

S. Bansal, S.B. Beri, V. Bhatnagar, S. Chauhan, R. Chawla, N. Dhingra, R. Gupta, A. Kaur, M. Kaur, S. Kaur, R. Kumar, P. Kumari, M. Lohan, A. Mehta, S. Sharma, J.B. Singh, G. Walia

University of Delhi, Delhi, India

A. Bhardwaj, B.C. Choudhary, R.B. Garg, S. Keshri, A. Kumar, Ashok Kumar, S. Malhotra, M. Naimuddin, K. Ranjan, Aashaq Shah, R. Sharma

Saha Institute of Nuclear Physics, HBNI, Kolkata, India

R. Bhardwaj²⁵, R. Bhattacharya, S. Bhattacharya, U. Bhawandeep²⁵, D. Bhowmik, S. Dey, S. Dutt²⁵, S. Dutta, S. Ghosh, N. Majumdar, K. Mondal, S. Mukhopadhyay, S. Nandan, A. Purohit, P.K. Rout, A. Roy, S. Roy Chowdhury, S. Sarkar, M. Sharan, B. Singh, S. Thakur²⁵

Indian Institute of Technology Madras, Madras, India

P.K. Behera

Bhabha Atomic Research Centre, Mumbai, India

R. Chudasama, D. Dutta, V. Jha, V. Kumar, A.K. Mohanty¹⁶, P.K. Netrakanti, L.M. Pant, P. Shukla, A. Topkar

Tata Institute of Fundamental Research-A, Mumbai, India

T. Aziz, S. Dugad, B. Mahakud, S. Mitra, G.B. Mohanty, N. Sur, B. Sutar

Tata Institute of Fundamental Research-B, Mumbai, India

S. Banerjee, S. Bhattacharya, S. Chatterjee, P. Das, M. Guchait, Sa. Jain, S. Kumar, M. Maity²⁶, G. Majumder, K. Mazumdar, N. Sahoo, T. Sarkar²⁶, N. Wickramage²⁷

Indian Institute of Science Education and Research (IISER), Pune, India

S. Chauhan, S. Dube, V. Hegde, A. Kapoor, K. Kothekar, S. Pandey, A. Rane, S. Sharma

Institute for Research in Fundamental Sciences (IPM), Tehran, Iran

S. Chenarani²⁸, E. Eskandari Tadavani, S.M. Etesami²⁸, M. Khakzad, M. Mohammadi Najafabadi, M. Naseri, S. Paktinat Mehdiabadi²⁹, F. Rezaei Hosseinabadi, B. Safarzadeh³⁰, M. Zeinali

University College Dublin, Dublin, Ireland

M. Felcini, M. Grunewald

INFN Sezione di Bari ^a, Università di Bari ^b, Politecnico di Bari ^c, Bari, Italy

M. Abbrescia^{a,b}, C. Calabria^{a,b}, A. Colaleo^a, D. Creanza^{a,c}, L. Cristella^{a,b}, N. De Filippis^{a,c}, M. De Palma^{a,b}, A. Di Florio^{a,b}, F. Errico^{a,b}, L. Fiore^a, A. Gelmi^{a,b}, G. Iaselli^{a,c}, S. Lezki^{a,b}, G. Maggi^{a,c}, M. Maggi^a, B. Marangelli^{a,b}, G. Miniello^{a,b}, S. My^{a,b}, S. Nuzzo^{a,b}, A. Pompili^{a,b}, G. Pugliese^{a,c}, R. Radogna^a, A. Ranieri^a, G. Selvaggi^{a,b}, A. Sharma^a, L. Silvestris^{a,16}, R. Venditti^a, P. Verwilligen^a, G. Zito^a

INFN Sezione di Bologna ^a, Università di Bologna ^b, Bologna, Italy

G. Abbiendi^a, C. Battilana^{a,b}, D. Bonacorsi^{a,b}, L. Borgonovi^{a,b}, S. Braibant-Giacomelli^{a,b},

L. Brigliadori^{a,b}, R. Campanini^{a,b}, P. Capiluppi^{a,b}, A. Castro^{a,b}, F.R. Cavallo^a, S.S. Chhibra^{a,b}, G. Codispoti^{a,b}, M. Cuffiani^{a,b}, G.M. Dallavalle^a, F. Fabbri^a, A. Fanfani^{a,b}, D. Fasanella^{a,b}, P. Giacomelli^a, C. Grandi^a, L. Guiducci^{a,b}, F. Iemmi, S. Marcellini^a, G. Masetti^a, A. Montanari^a, F.L. Navarra^{a,b}, A. Perrotta^a, T. Rovelli^{a,b}, G.P. Siroli^{a,b}, N. Tosi^a

INFN Sezione di Catania ^a, Università di Catania ^b, Catania, Italy

S. Albergo^{a,b}, S. Costa^{a,b}, A. Di Mattia^a, F. Giordano^{a,b}, R. Potenza^{a,b}, A. Tricomi^{a,b}, C. Tuve^{a,b}

INFN Sezione di Firenze ^a, Università di Firenze ^b, Firenze, Italy

G. Barbagli^a, K. Chatterjee^{a,b}, V. Ciulli^{a,b}, C. Civinini^a, R. D'Alessandro^{a,b}, E. Focardi^{a,b}, G. Latino, P. Lenzi^{a,b}, M. Meschini^a, S. Paoletti^a, L. Russo^{a,31}, G. Sguazzoni^a, D. Strom^a, L. Viliani^a

INFN Laboratori Nazionali di Frascati, Frascati, Italy

L. Benussi, S. Bianco, F. Fabbri, D. Piccolo, F. Primavera¹⁶

INFN Sezione di Genova ^a, Università di Genova ^b, Genova, Italy

V. Calvelli^{a,b}, F. Ferro^a, F. Ravera^{a,b}, E. Robutti^a, S. Tosi^{a,b}

INFN Sezione di Milano-Bicocca ^a, Università di Milano-Bicocca ^b, Milano, Italy

A. Benaglia^a, A. Beschi^b, L. Brianza^{a,b}, F. Brivio^{a,b}, V. Ciriolo^{a,b,16}, M.E. Dinardo^{a,b}, S. Fiorendi^{a,b}, S. Gennai^a, A. Ghezzi^{a,b}, P. Govoni^{a,b}, M. Malberti^{a,b}, S. Malvezzi^a, R.A. Manzoni^{a,b}, D. Menasce^a, L. Moroni^a, M. Paganoni^{a,b}, K. Pauwels^{a,b}, D. Pedrini^a, S. Pigazzini^{a,b,32}, S. Ragazzi^{a,b}, T. Tabarelli de Fatis^{a,b}

INFN Sezione di Napoli ^a, Università di Napoli 'Federico II' ^b, Napoli, Italy, Università della Basilicata ^c, Potenza, Italy, Università G. Marconi ^d, Roma, Italy

S. Buontempo^a, N. Cavallo^{a,c}, S. Di Guida^{a,d,16}, F. Fabozzi^{a,c}, F. Fienga^{a,b}, G. Galati^{a,b}, A.O.M. Iorio^{a,b}, W.A. Khan^a, L. Lista^a, S. Meola^{a,d,16}, P. Paolucci^{a,16}, C. Sciacca^{a,b}, F. Thyssen^a, E. Voevodina^{a,b}

INFN Sezione di Padova ^a, Università di Padova ^b, Padova, Italy, Università di Trento ^c, Trento, Italy

P. Azzi^a, N. Bacchetta^a, L. Benato^{a,b}, D. Bisello^{a,b}, A. Boletti^{a,b}, R. Carlin^{a,b}, A. Carvalho Antunes De Oliveira^{a,b}, P. Checchia^a, P. De Castro Manzano^a, T. Dorigo^a, U. Dosselli^a, F. Gasparini^{a,b}, U. Gasparini^{a,b}, A. Gozzelino^a, S. Lacaprara^a, M. Margoni^{a,b}, A.T. Meneguzzo^{a,b}, N. Pozzobon^{a,b}, P. Ronchese^{a,b}, R. Rossin^{a,b}, F. Simonetto^{a,b}, A. Tiko, E. Torassa^a, M. Zanetti^{a,b}, P. Zotto^{a,b}, G. Zumerle^{a,b}

INFN Sezione di Pavia ^a, Università di Pavia ^b, Pavia, Italy

A. Braghieri^a, A. Magnani^a, P. Montagna^{a,b}, S.P. Ratti^{a,b}, V. Re^a, M. Ressegotti^{a,b}, C. Riccardi^{a,b}, P. Salvini^a, I. Vai^{a,b}, P. Vitulo^{a,b}

INFN Sezione di Perugia ^a, Università di Perugia ^b, Perugia, Italy

L. Alunni Solestizi^{a,b}, M. Biasini^{a,b}, G.M. Bilei^a, C. Cecchi^{a,b}, D. Ciangottini^{a,b}, L. Fanò^{a,b}, P. Lariccia^{a,b}, R. Leonardi^{a,b}, E. Manoni^a, G. Mantovani^{a,b}, V. Mariani^{a,b}, M. Menichelli^a, A. Rossi^{a,b}, A. Santocchia^{a,b}, D. Spiga^a

INFN Sezione di Pisa ^a, Università di Pisa ^b, Scuola Normale Superiore di Pisa ^c, Pisa, Italy

K. Androsov^a, P. Azzurri^a, G. Bagliesi^a, L. Bianchini^a, T. Boccali^a, L. Borrello, R. Castaldi^a, M.A. Ciocci^{a,b}, R. Dell'Orso^a, G. Fedi^a, L. Giannini^{a,c}, A. Giassi^a, M.T. Grippo^a, F. Ligabue^{a,c}, T. Lomtadze^a, E. Manca^{a,c}, G. Mandorli^{a,c}, A. Messineo^{a,b}, F. Palla^a, A. Rizzi^{a,b}, P. Spagnolo^a, R. Tenchini^a, G. Tonelli^{a,b}, A. Venturi^a, P.G. Verdini^a

INFN Sezione di Roma ^a, Sapienza Università di Roma ^b, Rome, Italy

L. Barone^{a,b}, F. Cavallari^a, M. Cipriani^{a,b}, G. D'imperio^{a,b,16}, N. Daci^a, D. Del Re^{a,b}, E. Di Marco^{a,b}, M. Diemoz^a, S. Gelli^{a,b}, E. Longo^{a,b}, B. Marzocchi^{a,b}, P. Meridiani^a, G. Organtini^{a,b}, F. Pandolfi^a, R. Paramatti^{a,b}, F. Preiato^{a,b}, S. Rahatlou^{a,b}, C. Rovelli^a, F. Santanastasio^{a,b}

INFN Sezione di Torino ^a, Università di Torino ^b, Torino, Italy, Università del Piemonte Orientale ^c, Novara, Italy

N. Amapane^{a,b}, R. Arcidiacono^{a,c}, S. Argiro^{a,b}, M. Arneodo^{a,c}, N. Bartosik^a, R. Bellan^{a,b}, C. Biino^a, N. Cartiglia^a, R. Castello^{a,b}, F. Cenna^{a,b}, M. Costa^{a,b}, R. Covarelli^{a,b}, A. Degano^{a,b}, N. Demaria^a, B. Kiani^{a,b}, C. Mariotti^a, S. Maselli^a, E. Migliore^{a,b}, V. Monaco^{a,b}, E. Monteil^{a,b}, M. Monteno^a, M.M. Obertino^{a,b}, L. Pacher^{a,b}, N. Pastrone^a, M. Pelliccioni^a, G.L. Pinna Angioni^{a,b}, A. Romero^{a,b}, M. Ruspa^{a,c}, R. Sacchi^{a,b}, K. Shchelina^{a,b}, V. Sola^a, A. Solano^{a,b}, A. Staiano^a

INFN Sezione di Trieste ^a, Università di Trieste ^b, Trieste, Italy

S. Belforte^a, M. Casarsa^a, F. Cossutti^a, G. Della Ricca^{a,b}, A. Zanetti^a

Kyungpook National University

D.H. Kim, G.N. Kim, M.S. Kim, J. Lee, S. Lee, S.W. Lee, C.S. Moon, Y.D. Oh, S. Sekmen, D.C. Son, Y.C. Yang

Chonnam National University, Institute for Universe and Elementary Particles, Kwangju, Korea

H. Kim, D.H. Moon, G. Oh

Hanyang University, Seoul, Korea

J.A. Brochero Cifuentes, J. Goh, T.J. Kim

Korea University, Seoul, Korea

S. Cho, S. Choi, Y. Go, D. Gyun, S. Ha, B. Hong, Y. Jo, Y. Kim, K. Lee, K.S. Lee, S. Lee, J. Lim, S.K. Park, Y. Roh

Seoul National University, Seoul, Korea

J. Almond, J. Kim, J.S. Kim, H. Lee, K. Lee, K. Nam, S.B. Oh, B.C. Radburn-Smith, S.h. Seo, U.K. Yang, H.D. Yoo, G.B. Yu

University of Seoul, Seoul, Korea

H. Kim, J.H. Kim, J.S.H. Lee, I.C. Park

Sungkyunkwan University, Suwon, Korea

Y. Choi, C. Hwang, J. Lee, I. Yu

Vilnius University, Vilnius, Lithuania

V. Dudenias, A. Juodagalvis, J. Vaitkus

National Centre for Particle Physics, Universiti Malaya, Kuala Lumpur, Malaysia

I. Ahmed, Z.A. Ibrahim, M.A.B. Md Ali³³, F. Mohamad Idris³⁴, W.A.T. Wan Abdullah, M.N. Yusli, Z. Zolkapli

Centro de Investigacion y de Estudios Avanzados del IPN, Mexico City, Mexico

M.C. Duran-Osuna, H. Castilla-Valdez, E. De La Cruz-Burelo, G. Ramirez-Sanchez, I. Heredia-De La Cruz³⁵, R.I. Rabadan-Trejo, R. Lopez-Fernandez, J. Mejia Guisao, R. Reyes-Almanza, A. Sanchez-Hernandez

Universidad Iberoamericana, Mexico City, Mexico

S. Carrillo Moreno, C. Oropeza Barrera, F. Vazquez Valencia

Benemerita Universidad Autonoma de Puebla, Puebla, Mexico

J. Eysermans, I. Pedraza, H.A. Salazar Ibarguen, C. Uribe Estrada

Universidad Autónoma de San Luis Potosí, San Luis Potosí, Mexico

A. Morelos Pineda

University of Auckland, Auckland, New Zealand

D. Krofcheck

University of Canterbury, Christchurch, New Zealand

S. Bheesette, P.H. Butler

National Centre for Physics, Quaid-I-Azam University, Islamabad, Pakistan

A. Ahmad, M. Ahmad, Q. Hassan, H.R. Hoorani, A. Saddique, M.A. Shah, M. Shoaib, M. Waqas

National Centre for Nuclear Research, Swierk, Poland

H. Bialkowska, M. Bluj, B. Boimska, T. Frueboes, M. Górski, M. Kazana, K. Nawrocki, M. Szleper, P. Traczyk, P. Zalewski

Institute of Experimental Physics, Faculty of Physics, University of Warsaw, Warsaw, Poland

K. Bunkowski, A. Byzuk³⁶, K. Doroba, A. Kalinowski, M. Konecki, J. Krolikowski, M. Misiura, M. Olszewski, A. Pyskir, M. Walczak

Laboratório de Instrumentação e Física Experimental de Partículas, Lisboa, Portugal

P. Bargassa, C. Beirão Da Cruz E Silva, A. Di Francesco, P. Faccioli, B. Galinhas, M. Gallinaro, J. Hollar, N. Leonardo, L. Lloret Iglesias, M.V. Nemallapudi, J. Seixas, G. Strong, O. Toldaiev, D. Vadrucio, J. Varela

Joint Institute for Nuclear Research, Dubna, Russia

V. Alexakhin, A. Golunov, I. Golutvin, N. Gorbounov, I. Gorbunov, A. Kamenev, V. Karjavin, A. Lanev, A. Malakhov, V. Matveev^{37,38}, P. Moisenz, V. Palichik, V. Perelygin, M. Savina, S. Shmatov, S. Shulha, N. Skatchkov, V. Smirnov, A. Zarubin

Petersburg Nuclear Physics Institute, Gatchina (St. Petersburg), Russia

Y. Ivanov, V. Kim³⁹, E. Kuznetsova⁴⁰, P. Levchenko, V. Murzin, V. Oreshkin, I. Smirnov, D. Sosnov, V. Sulimov, L. Uvarov, S. Vavilov, A. Vorobyev

Institute for Nuclear Research, Moscow, Russia

Yu. Andreev, A. Dermenev, S. Gninenko, N. Golubev, A. Karneyeu, M. Kirsanov, N. Krasnikov, A. Pashenkov, D. Tlisov, A. Toropin

Institute for Theoretical and Experimental Physics, Moscow, Russia

V. Epshteyn, V. Gavrilov, N. Lychkovskaya, V. Popov, I. Pozdnyakov, G. Safronov, A. Spiridonov, A. Stepenov, V. Stolin, M. Toms, E. Vlasov, A. Zhokin

Moscow Institute of Physics and Technology, Moscow, Russia

T. Aushev, A. Bylinkin³⁸

National Research Nuclear University 'Moscow Engineering Physics Institute' (MEPhI), Moscow, Russia

M. Chadeeva⁴¹, P. Parygin, D. Philippov, S. Polikarpov, E. Popova, V. Rusinov

P.N. Lebedev Physical Institute, Moscow, Russia

V. Andreev, M. Azarkin³⁸, I. Dremin³⁸, M. Kirakosyan³⁸, S.V. Rusakov, A. Terkulov

Skobeltsyn Institute of Nuclear Physics, Lomonosov Moscow State University, Moscow, Russia

A. Baskakov, A. Belyaev, E. Boos, M. Dubinin⁴², L. Dudko, A. Ershov, A. Gribushin, V. Klyukhin, O. Kodolova, I. Lokhtin, I. Miagkov, S. Obraztsov, S. Petrushanko, V. Savrin, A. Snigirev

Novosibirsk State University (NSU), Novosibirsk, Russia

V. Blinov⁴³, D. Shtol⁴³, Y. Skovpen⁴³

State Research Center of Russian Federation, Institute for High Energy Physics of NRC “Kurchatov Institute”, Protvino, Russia

I. Azhgirey, I. Bayshev, S. Bitioukov, D. Elumakhov, A. Godizov, V. Kachanov, A. Kalinin, D. Konstantinov, P. Mandrik, V. Petrov, R. Ryutin, A. Sobol, S. Troshin, N. Tyurin, A. Uzunian, A. Volkov

National Research Tomsk Polytechnic University, Tomsk, Russia

A. Babaev

University of Belgrade, Faculty of Physics and Vinca Institute of Nuclear Sciences, Belgrade, Serbia

P. Adzic⁴⁴, P. Cirkovic, D. Devetak, M. Dordevic, J. Milosevic

Centro de Investigaciones Energéticas Medioambientales y Tecnológicas (CIEMAT), Madrid, Spain

J. Alcaraz Maestre, A. Álvarez Fernández, I. Bachiller, M. Barrio Luna, M. Cerrada, N. Colino, B. De La Cruz, A. Delgado Peris, C. Fernandez Bedoya, J.P. Fernández Ramos, J. Flix, M.C. Fouz, O. Gonzalez Lopez, S. Goy Lopez, J.M. Hernandez, M.I. Josa, D. Moran, A. Pérez-Calero Yzquierdo, J. Puerta Pelayo, I. Redondo, L. Romero, M.S. Soares, A. Triossi

Universidad Autónoma de Madrid, Madrid, Spain

C. Albajar, J.F. de Trocóniz

Universidad de Oviedo, Oviedo, Spain

J. Cuevas, C. Erice, J. Fernandez Menendez, S. Folgueras, I. Gonzalez Caballero, J.R. González Fernández, E. Palencia Cortezon, S. Sanchez Cruz, P. Vischia, J.M. Vizán García

Instituto de Física de Cantabria (IFCA), CSIC-Universidad de Cantabria, Santander, Spain

I.J. Cabrillo, A. Calderon, B. Chazin Quero, J. Duarte Campderros, M. Fernandez, P.J. Fernández Manteca, A. García Alonso, J. Garcia-Ferrero, G. Gomez, A. Lopez Virto, J. Marco, C. Martinez Rivero, P. Martinez Ruiz del Arbol, F. Matorras, J. Piedra Gomez, C. Prieels, T. Rodrigo, A. Ruiz-Jimeno, L. Scodellaro, N. Trevisani, I. Vila, R. Vilar Cortabitarte

CERN, European Organization for Nuclear Research, Geneva, Switzerland

D. Abbaneo, B. Akgun, E. Auffray, P. Baillon, A.H. Ball, D. Barney, J. Bendavid, M. Bianco, A. Bocci, C. Botta, T. Camporesi, M. Cepeda, G. Cerminara, E. Chapon, Y. Chen, D. d’Enterria, A. Dabrowski, V. Daponte, A. David, M. De Gruttola, A. De Roeck, N. Deelen, M. Dobson, T. du Pree, M. Dünser, N. Dupont, A. Elliott-Peisert, P. Everaerts, F. Fallavollita⁴⁵, G. Franzoni, J. Fulcher, W. Funk, D. Gigi, A. Gilbert, K. Gill, F. Glege, D. Gulhan, J. Hegeman, V. Innocente, A. Jafari, P. Janot, O. Karacheban¹⁹, J. Kieseler, V. Knünz, A. Kornmayer, M. Krammer¹, C. Lange, P. Lecoq, C. Lourenço, M.T. Lucchini, L. Malgeri, M. Mannelli, A. Martelli, F. Meijers, J.A. Merlin, S. Mersi, E. Meschi, P. Milenovic⁴⁶, F. Moortgat, M. Mulders, H. Neugebauer, J. Ngadiuba, S. Orfanelli, L. Orsini, F. Pantaleo¹⁶, L. Pape, E. Perez, M. Peruzzi, A. Petrilli, G. Petrucciani, A. Pfeiffer, M. Pierini, F.M. Pitters, D. Rabady, A. Racz, T. Reis, G. Rolandi⁴⁷, M. Rovere, H. Sakulin, C. Schäfer, C. Schwick, M. Seidel, M. Selvaggi, A. Sharma, P. Silva,

P. Sphicas⁴⁸, A. Stakia, J. Steggemann, M. Stoye, M. Tosi, D. Treille, A. Tsirou, V. Veckalns⁴⁹, M. Verweij, W.D. Zeuner

Paul Scherrer Institut, Villigen, Switzerland

W. Bertl[†], L. Caminada⁵⁰, K. Deiters, W. Erdmann, R. Horisberger, Q. Ingram, H.C. Kaestli, D. Kotlinski, U. Langenegger, T. Rohe, S.A. Wiederkehr

ETH Zurich - Institute for Particle Physics and Astrophysics (IPA), Zurich, Switzerland

M. Backhaus, L. Bäni, P. Berger, B. Casal, N. Chernyavskaya, G. Dissertori, M. Dittmar, M. Donegà, C. Dorfer, C. Grab, C. Heidegger, D. Hits, J. Hoss, T. Klijnsma, W. Luster, M. Marionneau, M.T. Meinhard, D. Meister, F. Micheli, P. Musella, F. Nessi-Tedaldi, J. Pata, F. Pauss, G. Perrin, L. Perrozzi, M. Quittnat, M. Reichmann, D. Ruini, D.A. Sanz Becerra, M. Schönenberger, L. Shchutska, V.R. Tavolaro, K. Theofilatos, M.L. Vesterbacka Olsson, R. Wallny, D.H. Zhu

Universität Zürich, Zurich, Switzerland

T.K. Aarrestad, C. Amsler⁵¹, D. Brzhechko, M.F. Canelli, A. De Cosa, R. Del Burgo, S. Donato, C. Galloni, T. Hreus, B. Kilminster, I. Neutelings, D. Pinna, G. Rauco, P. Robmann, D. Salerno, K. Schweiger, C. Seitz, Y. Takahashi, A. Zucchetta

National Central University, Chung-Li, Taiwan

V. Candelise, Y.H. Chang, K.y. Cheng, T.H. Doan, Sh. Jain, R. Khurana, C.M. Kuo, W. Lin, A. Pozdnyakov, S.S. Yu

National Taiwan University (NTU), Taipei, Taiwan

P. Chang, Y. Chao, K.F. Chen, P.H. Chen, F. Fiori, W.-S. Hou, Y. Hsiung, Arun Kumar, Y.F. Liu, R.-S. Lu, E. Paganis, A. Psallidas, A. Steen, J.f. Tsai

Chulalongkorn University, Faculty of Science, Department of Physics, Bangkok, Thailand

B. Asavapibhop, K. Kovitanggoon, G. Singh, N. Srimanobhas

Çukurova University, Physics Department, Science and Art Faculty, Adana, Turkey

M.N. Bakirci⁵², A. Bat, F. Boran, S. Cerci⁵³, S. Damarseckin, Z.S. Demiroglu, C. Dozen, I. Dumanoglu, S. Girgis, G. Gokbulut, Y. Guler, I. Hos⁵⁴, E.E. Kangal⁵⁵, O. Kara, A. Kayis Topaksu, U. Kiminsu, M. Oglakci, G. Onengut, K. Ozdemir⁵⁶, B. Tali⁵³, U.G. Tok, S. Turkcapar, I.S. Zorbakir, C. Zorbilmez

Middle East Technical University, Physics Department, Ankara, Turkey

G. Karapinar⁵⁷, K. Ocalan⁵⁸, M. Yalvac, M. Zeyrek

Bogazici University, Istanbul, Turkey

I.O. Atakisi, E. Gülmez, M. Kaya⁵⁹, O. Kaya⁶⁰, S. Tekten, E.A. Yetkin⁶¹

Istanbul Technical University, Istanbul, Turkey

M.N. Agaras, S. Atay, A. Cakir, K. Cankocak, Y. Komurcu

Institute for Scintillation Materials of National Academy of Science of Ukraine, Kharkov, Ukraine

B. Grynyov

National Scientific Center, Kharkov Institute of Physics and Technology, Kharkov, Ukraine

L. Levchuk

University of Bristol, Bristol, United Kingdom

F. Ball, L. Beck, J.J. Brooke, D. Burns, E. Clement, D. Cussans, O. Davignon, H. Flacher,

J. Goldstein, G.P. Heath, H.F. Heath, L. Kreczko, D.M. Newbold⁶², S. Paramesvaran, T. Sakuma, S. Seif El Nasr-storey, D. Smith, V.J. Smith

Rutherford Appleton Laboratory, Didcot, United Kingdom

K.W. Bell, A. Belyaev⁶³, C. Brew, R.M. Brown, D. Cieri, D.J.A. Cockerill, J.A. Coughlan, K. Harder, S. Harper, J. Linacre, E. Olaiya, D. Petyt, C.H. Shepherd-Themistocleous, A. Thea, I.R. Tomalin, T. Williams, W.J. Womersley

Imperial College, London, United Kingdom

G. Auzinger, R. Bainbridge, P. Bloch, J. Borg, S. Breeze, O. Buchmuller, A. Bundock, S. Casasso, D. Colling, L. Corpe, P. Dauncey, G. Davies, M. Della Negra, R. Di Maria, Y. Haddad, G. Hall, G. Iles, T. James, M. Komm, R. Lane, C. Laner, L. Lyons, A.-M. Magnan, S. Malik, L. Mastrolorenzo, T. Matsushita, J. Nash⁶⁴, A. Nikitenko⁷, V. Palladino, M. Pesaresi, A. Richards, A. Rose, E. Scott, C. Seez, A. Shtipliyski, T. Strebler, S. Summers, A. Tapper, K. Uchida, M. Vazquez Acosta⁶⁵, T. Virdee¹⁶, N. Wardle, D. Winterbottom, J. Wright, S.C. Zenz

Brunel University, Uxbridge, United Kingdom

J.E. Cole, P.R. Hobson, A. Khan, P. Kyberd, A. Morton, I.D. Reid, L. Teodorescu, S. Zahid

Baylor University, Waco, USA

A. Borzou, K. Call, J. Dittmann, K. Hatakeyama, H. Liu, N. Pastika, C. Smith

Catholic University of America, Washington DC, USA

R. Bartek, A. Dominguez

The University of Alabama, Tuscaloosa, USA

A. Buccilli, S.I. Cooper, C. Henderson, P. Rumerio, C. West

Boston University, Boston, USA

D. Arcaro, A. Avetisyan, T. Bose, D. Gastler, D. Rankin, C. Richardson, J. Rohlf, L. Sulak, D. Zou

Brown University, Providence, USA

G. Benelli, D. Cutts, M. Hadley, J. Hakala, U. Heintz, J.M. Hogan⁶⁶, K.H.M. Kwok, E. Laird, G. Landsberg, J. Lee, Z. Mao, M. Narain, J. Pazzini, S. Piperov, S. Sagir, R. Syarif, D. Yu

University of California, Davis, Davis, USA

R. Band, C. Brainerd, R. Breedon, D. Burns, M. Calderon De La Barca Sanchez, M. Chertok, J. Conway, R. Conway, P.T. Cox, R. Erbacher, C. Flores, G. Funk, W. Ko, R. Lander, C. Mclean, M. Mulhearn, D. Pellett, J. Pilot, S. Shalhout, M. Shi, J. Smith, D. Stolp, D. Taylor, K. Tos, M. Tripathi, Z. Wang, F. Zhang

University of California, Los Angeles, USA

M. Bachtis, C. Bravo, R. Cousins, A. Dasgupta, A. Florent, J. Hauser, M. Ignatenko, N. Mccoll, S. Regnard, D. Saltzberg, C. Schnaible, V. Valuev

University of California, Riverside, Riverside, USA

E. Bouvier, K. Burt, R. Clare, J. Ellison, J.W. Gary, S.M.A. Ghiasi Shirazi, G. Hanson, G. Karapostoli, E. Kennedy, F. Lacroix, O.R. Long, M. Olmedo Negrete, M.I. Paneva, W. Si, L. Wang, H. Wei, S. Wimpenny, B.R. Yates

University of California, San Diego, La Jolla, USA

J.G. Branson, S. Cittolin, M. Derdzinski, R. Gerosa, D. Gilbert, B. Hashemi, A. Holzner, D. Klein, G. Kole, V. Krutelyov, J. Letts, M. Masciovecchio, D. Olivito, S. Padhi, M. Pieri, M. Sani, V. Sharma, S. Simon, M. Tadel, A. Vartak, S. Wasserbaech⁶⁷, J. Wood, F. Würthwein, A. Yagil, G. Zevi Della Porta

University of California, Santa Barbara - Department of Physics, Santa Barbara, USA

N. Amin, R. Bhandari, J. Bradmiller-Feld, C. Campagnari, M. Citron, A. Dishaw, V. Dutta, M. Franco Sevilla, L. Gouskos, R. Heller, J. Incandela, A. Ovcharova, H. Qu, J. Richman, D. Stuart, I. Suarez, J. Yoo

California Institute of Technology, Pasadena, USA

D. Anderson, A. Bornheim, J. Bunn, J.M. Lawhorn, H.B. Newman, T.Q. Nguyen, C. Pena, M. Spiropulu, J.R. Vlimant, R. Wilkinson, S. Xie, Z. Zhang, R.Y. Zhu

Carnegie Mellon University, Pittsburgh, USA

M.B. Andrews, T. Ferguson, T. Mudholkar, M. Paulini, J. Russ, M. Sun, H. Vogel, I. Vorobiev, M. Weinberg

University of Colorado Boulder, Boulder, USA

J.P. Cumalat, W.T. Ford, F. Jensen, A. Johnson, M. Krohn, S. Leontsinis, E. MacDonald, T. Mulholland, K. Stenson, K.A. Ulmer, S.R. Wagner

Cornell University, Ithaca, USA

J. Alexander, J. Chaves, Y. Cheng, J. Chu, A. Datta, K. Mcdermott, N. Mirman, J.R. Patterson, D. Quach, A. Rinkevicius, A. Ryd, L. Skinnari, L. Soffi, S.M. Tan, Z. Tao, J. Thom, J. Tucker, P. Wittich, M. Zientek

Fermi National Accelerator Laboratory, Batavia, USA

S. Abdullin, M. Albrow, M. Alyari, G. Apollinari, A. Apresyan, A. Apyan, S. Banerjee, L.A.T. Bauerdick, A. Beretvas, J. Berryhill, P.C. Bhat, G. Bolla[†], K. Burkett, J.N. Butler, A. Canepa, G.B. Cerati, H.W.K. Cheung, F. Chlebana, M. Cremonesi, J. Duarte, V.D. Elvira, J. Freeman, Z. Gecse, E. Gottschalk, L. Gray, D. Green, S. Grünendahl, O. Gutsche, J. Hanlon, R.M. Harris, S. Hasegawa, J. Hirschauer, Z. Hu, B. Jayatilaka, S. Jindariani, M. Johnson, U. Joshi, B. Klima, M.J. Kortelainen, B. Kreis, S. Lammel, D. Lincoln, R. Lipton, M. Liu, T. Liu, R. Lopes De Sá, J. Lykken, K. Maeshima, N. Magini, J.M. Marraffino, D. Mason, P. McBride, P. Merkel, S. Mrenna, S. Nahn, V. O'Dell, K. Pedro, O. Prokofyev, G. Rakness, L. Ristori, A. Savoy-Navarro⁶⁸, B. Schneider, E. Sexton-Kennedy, A. Soha, W.J. Spalding, L. Spiegel, S. Stoynev, J. Strait, N. Strobbe, L. Taylor, S. Tkaczyk, N.V. Tran, L. Uplegger, E.W. Vaandering, C. Vernieri, M. Verzocchi, R. Vidal, M. Wang, H.A. Weber, A. Whitbeck, W. Wu

University of Florida, Gainesville, USA

D. Acosta, P. Avery, P. Bortignon, D. Bourilkov, A. Brinkerhoff, A. Carnes, M. Carver, D. Curry, R.D. Field, I.K. Furic, S.V. Gleyzer, B.M. Joshi, J. Konigsberg, A. Korytov, K. Kotov, P. Ma, K. Matchev, H. Mei, G. Mitselmakher, K. Shi, D. Sperka, N. Terentyev, L. Thomas, J. Wang, S. Wang, J. Yelton

Florida International University, Miami, USA

Y.R. Joshi, S. Linn, P. Markowitz, J.L. Rodriguez

Florida State University, Tallahassee, USA

A. Ackert, T. Adams, A. Askew, S. Hagopian, V. Hagopian, K.F. Johnson, T. Kolberg, G. Martinez, T. Perry, H. Prosper, A. Saha, A. Santra, V. Sharma, R. Yohay

Florida Institute of Technology, Melbourne, USA

M.M. Baarmand, V. Bhopatkar, S. Colafranceschi, M. Hohlmann, D. Noonan, T. Roy, F. Yumiceva

University of Illinois at Chicago (UIC), Chicago, USA

M.R. Adams, L. Apanasevich, D. Berry, R.R. Betts, R. Cavanaugh, X. Chen, S. Dittmer,

O. Evdokimov, C.E. Gerber, D.A. Hangal, D.J. Hofman, K. Jung, J. Kamin, I.D. Sandoval Gonzalez, M.B. Tonjes, N. Varelas, H. Wang, Z. Wu, J. Zhang

The University of Iowa, Iowa City, USA

B. Bilki⁶⁹, W. Clarida, K. Dilsiz⁷⁰, S. Durgut, R.P. Gandrajula, M. Haytmyradov, V. Khristenko, J.-P. Merlo, H. Mermerkaya⁷¹, A. Mestvirishvili, A. Moeller, J. Nachtman, H. Ogul⁷², Y. Onel, F. Ozok⁷³, A. Penzo, C. Snyder, E. Tiras, J. Wetzel, K. Yi

Johns Hopkins University, Baltimore, USA

B. Blumenfeld, A. Cocoros, N. Eminizer, D. Fehling, L. Feng, A.V. Gritsan, W.T. Hung, P. Maksimovic, J. Roskes, U. Sarica, M. Swartz, M. Xiao, C. You

The University of Kansas, Lawrence, USA

A. Al-bataineh, P. Baringer, A. Bean, S. Boren, J. Bowen, J. Castle, S. Khalil, A. Kropivnitskaya, D. Majumder, W. Mcbrayer, M. Murray, C. Rogan, C. Royon, S. Sanders, E. Schmitz, J.D. Tapia Takaki, Q. Wang

Kansas State University, Manhattan, USA

A. Ivanov, K. Kaadze, Y. Maravin, A. Modak, A. Mohammadi, L.K. Saini, N. Skhirtladze

Lawrence Livermore National Laboratory, Livermore, USA

F. Rebassoo, D. Wright

University of Maryland, College Park, USA

A. Baden, O. Baron, A. Belloni, S.C. Eno, Y. Feng, C. Ferraioli, N.J. Hadley, S. Jabeen, G.Y. Jeng, R.G. Kellogg, J. Kunkle, A.C. Mignerey, F. Ricci-Tam, Y.H. Shin, A. Skuja, S.C. Tonwar

Massachusetts Institute of Technology, Cambridge, USA

D. Abercrombie, B. Allen, V. Azzolini, R. Barbieri, A. Baty, G. Bauer, R. Bi, S. Brandt, W. Busza, I.A. Cali, M. D'Alfonso, Z. Demiragli, G. Gomez Ceballos, M. Goncharov, P. Harris, D. Hsu, M. Hu, Y. Iiyama, G.M. Innocenti, M. Klute, D. Kovalskyi, Y.-J. Lee, A. Levin, P.D. Luckey, B. Maier, A.C. Marini, C. McGinn, C. Mironov, S. Narayanan, X. Niu, C. Paus, C. Roland, G. Roland, G.S.F. Stephans, K. Sumorok, K. Tatar, D. Velicanu, J. Wang, T.W. Wang, B. Wyslouch, S. Zhaozhong

University of Minnesota, Minneapolis, USA

A.C. Benvenuti, R.M. Chatterjee, A. Evans, P. Hansen, S. Kalafut, Y. Kubota, Z. Lesko, J. Mans, S. Nourbakhsh, N. Ruckstuhl, R. Rusack, J. Turkewitz, M.A. Wadud

University of Mississippi, Oxford, USA

J.G. Acosta, S. Oliveros

University of Nebraska-Lincoln, Lincoln, USA

E. Avdeeva, K. Bloom, D.R. Claes, C. Fangmeier, F. Golf, R. Gonzalez Suarez, R. Kamalieddin, I. Kravchenko, J. Monroy, J.E. Siado, G.R. Snow, B. Stieger

State University of New York at Buffalo, Buffalo, USA

A. Godshalk, C. Harrington, I. Iashvili, D. Nguyen, A. Parker, S. Rappoccio, B. Roozbahani

Northeastern University, Boston, USA

G. Alverson, E. Barberis, C. Freer, A. Hortiangtham, A. Massironi, D.M. Morse, T. Orimoto, R. Teixeira De Lima, T. Wamorkar, B. Wang, A. Wisecarver, D. Wood

Northwestern University, Evanston, USA

S. Bhattacharya, O. Charaf, K.A. Hahn, N. Mucia, N. Odell, M.H. Schmitt, K. Sung, M. Trovato, M. Velasco

University of Notre Dame, Notre Dame, USA

R. Bucci, N. Dev, M. Hildreth, K. Hurtado Anampa, C. Jessop, D.J. Karmgard, N. Kellams, K. Lannon, W. Li, N. Loukas, N. Marinelli, F. Meng, C. Mueller, Y. Musienko³⁷, M. Planer, A. Reinsvold, R. Ruchti, P. Siddireddy, G. Smith, S. Taroni, M. Wayne, A. Wightman, M. Wolf, A. Woodard

The Ohio State University, Columbus, USA

J. Alimena, L. Antonelli, B. Bylsma, L.S. Durkin, S. Flowers, B. Francis, A. Hart, C. Hill, W. Ji, T.Y. Ling, W. Luo, B.L. Winer, H.W. Wulsin

Princeton University, Princeton, USA

S. Cooperstein, O. Driga, P. Elmer, J. Hardenbrook, P. Hebda, S. Higginbotham, A. Kalogeropoulos, D. Lange, J. Luo, D. Marlow, K. Mei, I. Ojalvo, J. Olsen, C. Palmer, P. Piroué, J. Salfeld-Nebgen, D. Stickland, C. Tully

University of Puerto Rico, Mayaguez, USA

S. Malik, S. Norberg

Purdue University, West Lafayette, USA

A. Barker, V.E. Barnes, S. Das, L. Gutay, M. Jones, A.W. Jung, A. Khatiwada, D.H. Miller, N. Neumeister, C.C. Peng, H. Qiu, J.F. Schulte, J. Sun, F. Wang, R. Xiao, W. Xie

Purdue University Northwest, Hammond, USA

T. Cheng, J. Dolen, N. Parashar

Rice University, Houston, USA

Z. Chen, K.M. Ecklund, S. Freed, F.J.M. Geurts, M. Guilbaud, M. Kilpatrick, W. Li, B. Michlin, B.P. Padley, J. Roberts, J. Rorie, W. Shi, Z. Tu, J. Zabel, A. Zhang

University of Rochester, Rochester, USA

A. Bodek, P. de Barbaro, R. Demina, Y.t. Duh, T. Ferbel, M. Galanti, A. Garcia-Bellido, J. Han, O. Hindrichs, A. Khukhunaishvili, K.H. Lo, P. Tan, M. Verzetti

The Rockefeller University, New York, USA

R. Ciesielski, K. Goulianos, C. Mesropian

Rutgers, The State University of New Jersey, Piscataway, USA

A. Agapitos, J.P. Chou, Y. Gershtein, T.A. Gómez Espinosa, E. Halkiadakis, M. Heindl, E. Hughes, S. Kaplan, R. Kunnawalkam Elayavalli, S. Kyriacou, A. Lath, R. Montalvo, K. Nash, M. Osherson, H. Saka, S. Salur, S. Schnetzer, D. Sheffield, S. Somalwar, R. Stone, S. Thomas, P. Thomassen, M. Walker

University of Tennessee, Knoxville, USA

A.G. Delannoy, J. Heideman, G. Riley, K. Rose, S. Spanier, K. Thapa

Texas A&M University, College Station, USA

O. Bouhali⁷⁴, A. Castaneda Hernandez⁷⁴, A. Celik, M. Dalchenko, M. De Mattia, A. Delgado, S. Dildick, R. Eusebi, J. Gilmore, T. Huang, T. Kamon⁷⁵, R. Mueller, Y. Pakhotin, R. Patel, A. Perloff, L. Perniè, D. Rathjens, A. Safonov, A. Tatarinov

Texas Tech University, Lubbock, USA

N. Akchurin, J. Damgov, F. De Guio, P.R. Duderov, J. Faulkner, E. Gurpinar, S. Kunori, K. Lamichhane, S.W. Lee, T. Mengke, S. Muthumuni, T. Peltola, S. Undleeb, I. Volobouev, Z. Wang

Vanderbilt University, Nashville, USA

S. Greene, A. Gurrola, R. Janjam, W. Johns, C. Maguire, A. Melo, H. Ni, K. Padeken, J.D. Ruiz Alvarez, P. Sheldon, S. Tuo, J. Velkovska, Q. Xu

University of Virginia, Charlottesville, USA

M.W. Arenton, P. Barria, B. Cox, R. Hirosky, M. Joyce, A. Ledovskoy, H. Li, C. Neu, T. Sinthuprasith, Y. Wang, E. Wolfe, F. Xia

Wayne State University, Detroit, USA

R. Harr, P.E. Karchin, N. Poudyal, J. Sturdy, P. Thapa, S. Zaleski

University of Wisconsin - Madison, Madison, WI, USA

M. Brodski, J. Buchanan, C. Caillol, D. Carlsmith, S. Dasu, L. Dodd, S. Duric, B. Gomber, M. Grothe, M. Herndon, A. Hervé, U. Hussain, P. Klabbers, A. Lanaro, A. Levine, K. Long, R. Loveless, V. Rekovic, T. Ruggles, A. Savin, N. Smith, W.H. Smith, N. Woods

†: Deceased

1: Also at Vienna University of Technology, Vienna, Austria

2: Also at IRFU, CEA, Université Paris-Saclay, Gif-sur-Yvette, France

3: Also at Universidade Estadual de Campinas, Campinas, Brazil

4: Also at Federal University of Rio Grande do Sul, Porto Alegre, Brazil

5: Also at Universidade Federal de Pelotas, Pelotas, Brazil

6: Also at Université Libre de Bruxelles, Bruxelles, Belgium

7: Also at Institute for Theoretical and Experimental Physics, Moscow, Russia

8: Also at Joint Institute for Nuclear Research, Dubna, Russia

9: Also at Suez University, Suez, Egypt

10: Now at British University in Egypt, Cairo, Egypt

11: Also at Zewail City of Science and Technology, Zewail, Egypt

12: Also at Department of Physics, King Abdulaziz University, Jeddah, Saudi Arabia

13: Also at Université de Haute Alsace, Mulhouse, France

14: Also at Skobeltsyn Institute of Nuclear Physics, Lomonosov Moscow State University, Moscow, Russia

15: Also at Tbilisi State University, Tbilisi, Georgia

16: Also at CERN, European Organization for Nuclear Research, Geneva, Switzerland

17: Also at RWTH Aachen University, III. Physikalisches Institut A, Aachen, Germany

18: Also at University of Hamburg, Hamburg, Germany

19: Also at Brandenburg University of Technology, Cottbus, Germany

20: Also at Institute of Nuclear Research ATOMKI, Debrecen, Hungary

21: Also at MTA-ELTE Lendület CMS Particle and Nuclear Physics Group, Eötvös Loránd University, Budapest, Hungary

22: Also at Institute of Physics, University of Debrecen, Debrecen, Hungary

23: Also at Indian Institute of Technology Bhubaneswar, Bhubaneswar, India

24: Also at Institute of Physics, Bhubaneswar, India

25: Also at Shoolini University, Solan, India

26: Also at University of Visva-Bharati, Santiniketan, India

27: Also at University of Ruhuna, Matara, Sri Lanka

28: Also at Isfahan University of Technology, Isfahan, Iran

29: Also at Yazd University, Yazd, Iran

30: Also at Plasma Physics Research Center, Science and Research Branch, Islamic Azad University, Tehran, Iran

31: Also at Università degli Studi di Siena, Siena, Italy

- 32: Also at INFN Sezione di Milano-Bicocca ^a, Università di Milano-Bicocca ^b, Milano, Italy
- 33: Also at International Islamic University of Malaysia, Kuala Lumpur, Malaysia
- 34: Also at Malaysian Nuclear Agency, MOSTI, Kajang, Malaysia
- 35: Also at Consejo Nacional de Ciencia y Tecnología, Mexico city, Mexico
- 36: Also at Warsaw University of Technology, Institute of Electronic Systems, Warsaw, Poland
- 37: Also at Institute for Nuclear Research, Moscow, Russia
- 38: Now at National Research Nuclear University 'Moscow Engineering Physics Institute' (MEPhI), Moscow, Russia
- 39: Also at St. Petersburg State Polytechnical University, St. Petersburg, Russia
- 40: Also at University of Florida, Gainesville, USA
- 41: Also at P.N. Lebedev Physical Institute, Moscow, Russia
- 42: Also at California Institute of Technology, Pasadena, USA
- 43: Also at Budker Institute of Nuclear Physics, Novosibirsk, Russia
- 44: Also at Faculty of Physics, University of Belgrade, Belgrade, Serbia
- 45: Also at INFN Sezione di Pavia ^a, Università di Pavia ^b, Pavia, Italy
- 46: Also at University of Belgrade, Faculty of Physics and Vinca Institute of Nuclear Sciences, Belgrade, Serbia
- 47: Also at Scuola Normale e Sezione dell'INFN, Pisa, Italy
- 48: Also at National and Kapodistrian University of Athens, Athens, Greece
- 49: Also at Riga Technical University, Riga, Latvia
- 50: Also at Universität Zürich, Zurich, Switzerland
- 51: Also at Stefan Meyer Institute for Subatomic Physics (SMI), Vienna, Austria
- 52: Also at Gaziosmanpasa University, Tokat, Turkey
- 53: Also at Adiyaman University, Adiyaman, Turkey
- 54: Also at Istanbul Aydin University, Istanbul, Turkey
- 55: Also at Mersin University, Mersin, Turkey
- 56: Also at Piri Reis University, Istanbul, Turkey
- 57: Also at Izmir Institute of Technology, Izmir, Turkey
- 58: Also at Necmettin Erbakan University, Konya, Turkey
- 59: Also at Marmara University, Istanbul, Turkey
- 60: Also at Kafkas University, Kars, Turkey
- 61: Also at Istanbul Bilgi University, Istanbul, Turkey
- 62: Also at Rutherford Appleton Laboratory, Didcot, United Kingdom
- 63: Also at School of Physics and Astronomy, University of Southampton, Southampton, United Kingdom
- 64: Also at Monash University, Faculty of Science, Clayton, Australia
- 65: Also at Instituto de Astrofísica de Canarias, La Laguna, Spain
- 66: Also at Bethel University, St. Paul, USA
- 67: Also at Utah Valley University, Orem, USA
- 68: Also at Purdue University, West Lafayette, USA
- 69: Also at Beykent University, Istanbul, Turkey
- 70: Also at Bingol University, Bingol, Turkey
- 71: Also at Erzincan University, Erzincan, Turkey
- 72: Also at Sinop University, Sinop, Turkey
- 73: Also at Mimar Sinan University, Istanbul, Istanbul, Turkey
- 74: Also at Texas A&M University at Qatar, Doha, Qatar
- 75: Also at Kyungpook National University, Daegu, Korea